BIOCHEMISTRY
including biophysical chemistry & molecular biology

Article

pubs.acs.org/biochemistry

Structure and Catalysis in the *Escherichia coli* Hotdog-fold Thioesterase Paralogs YdiI and YbdB

Rui Wu,[†,§] John A. Latham,[‡,§] Danqi Chen,[‡] Jeremiah Farelli,[†] Hong Zhao,[‡] Kaila Matthews,[‡] Karen N. Allen,*[,†] and Debra Dunaway-Mariano*[,‡]

[†]Department of Chemistry, Boston University, Boston, Massachusetts 02215, United States

[‡]Department of Chemistry & Chemical Biology, University of New Mexico, Albuquerque, New Mexico 87131, United States

Supporting Information

ABSTRACT: Herein, the structural determinants for substrate recognition and catalysis in two hotdog-fold thioesterase paralogs, YbdB and YdiI from *Escherichia coli*, are identified and analyzed to provide insight into the evolution of biological function in the hotdog-fold enzyme superfamily. The X-ray crystal structures of YbdB and YdiI, in complex with inert substrate analogs, determined in this study revealed the locations of the respective thioester substrate binding sites and the identity of the residues positioned for substrate binding and catalysis. The importance of each of these residues was assessed through amino acid replacements followed by steady-state kinetic analyses of the corresponding site-directed mutants. Transient kinetic and solvent ^{18}O-labeling studies were then carried out to provide insight into the role of Glu63 posited to function as the nucleophile or general base in catalysis. Finally, the structure−function−mechanism profiles of the two paralogs, along with that of a more distant homolog, were compared to identify conserved elements of substrate recognition and catalysis, which define the core traits of the hotdog-fold thioesterase family, as well as structural features that are unique to each thioesterase. Founded on the insight gained from this analysis, we conclude that the promiscuity revealed by *in vitro* substrate activity determinations, and posited to facilitate the evolution of new biological function, is the product of intrinsic plasticity in substrate binding as well as in the catalytic mechanism.

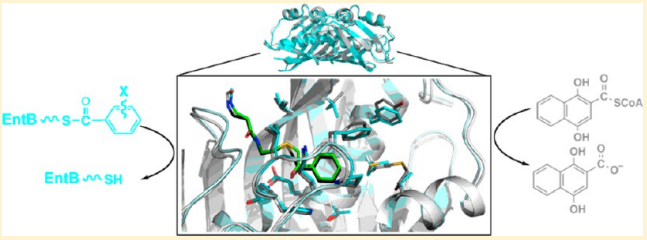

The hotdog-fold superfamily is a functionally diverse family of evolutionarily related enzymes, which share a common $\alpha + \beta$-fold. The founding member of this superfamily is the *Escherichia coli* β-hydroxydecanoyl-*holo* acyl carrier protein (ACP) dehydrase/isomerase.[a5] Smith and co-workers coined the name "hotdog-fold" to represent the observed tertiary structure consisting of a 5-turn α-helix cradled by a curved, 7-stranded antiparallel β-sheet. The functional unit was reported as a dimer, with the subunit interface joining the two sheets into a continuous 14-stranded β-sheet. The two active sites are located at opposite ends of the interfaced sheets.

Soon after the report of the dehydratase/isomerase, the hotdog-fold was observed in the 4-hydroxybenzoyl-coenzyme A thioesterase from *Pseudomonas* sp. strain CBS3 (*Ps* 4-HB-CoA TE)[1] and shortly thereafter in the 4-HB-CoA thioesterase from *Arthrobacter* special strain AU (*Ar* 4-HB-CoA TE)[3] (Figure 1A and B). Both thioesterases catalyze the final step of the 4-chlorobenzoate-degradation pathway.[6,7] Surprisingly, the two thioesterases share little sequence identity (<25%), and although the tertiary structures are alike, the arrangements of the dimers, which form the respective (biological unit) tetramers, differ. Specifically, the dimers of the *Ar* 4-HB-CoA TE associate β-sheet-to-β-sheet, with the active sites directed to solvent, whereas in the *Ps* 4-HB-CoA TE structure the dimers are rotated 180° such that the active sites are directed to the dimer−dimer interface.[1−3]

Most relevant to the catalytic mechanism is the fact that even though the secondary structural elements that form the active sites of the two thioesterases are highly conserved, the constellation of catalytic residues is dissimilar as is the spatial location of the essential catalytic carboxylate residue.[2,3] Based on the noted structural differences, the *Ar* 4-HB-CoA TE and *Ps* 4-HB-CoA TE are viewed as prototypes of two evolutionarily distinct clades of thioesterases within the hotdog-fold superfamily.[b] Notably, the common fold that links these two structural clades dictates that, for all members, substrate recognition is directed at *holo*ACP or CoA-based thioester metabolites.

The thioesterases constitute a large subfamily within the hotdog-fold superfamily. The biological function of the thioesterase is defined by the identity of its *in vivo* substrate(s) (i.e., physiological substrate(s)) in combination with the biochemical context, as determined by protein partners and/or elements of regulation. When subjected to an *in vitro* activity screen, the typical hotdog-fold thioesterase displays hydrolytic activities toward a range of thioesters that extend well beyond the physiological substrate(s).[8−12] Whereas this lack of substrate specificity might, in earlier times, have been

Received: March 18, 2014
Revised: July 2, 2014
Published: July 3, 2014

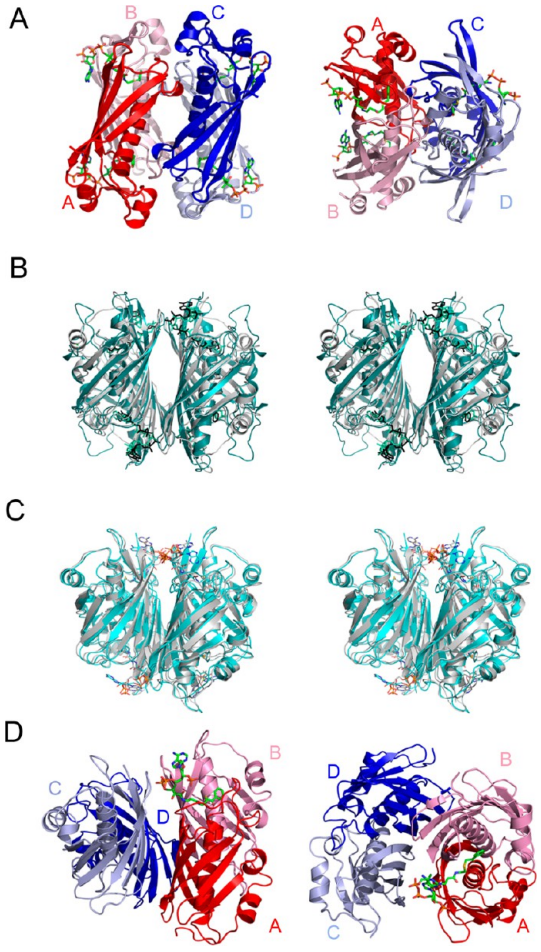

Figure 1. (A) Tetrameric structure (dimer of dimers) of the hotdog-fold superfamily clade AA member 4-hydroxybenzoyl-CoA thioesterase from *Pseudomonas* sp. strain CBS3 represented in Pymol.[2] The two structural representations are related by a 90° vertical rotation. The red and pink subunits comprise one dimer, and the light blue and royal blue subunits comprise the other dimer. The inert substrate analog, 4-hydroxyphenacyl-CoA (shown in stick with green carbon atoms, red oxygen atoms, blue nitrogen atoms, and a yellow sulfur atom), is bound to each of the four active sites. (B) Pymol stereo representation of the superposition of the tetrameric structures (dimer of dimers) of the hotdog-fold superfamily clade AB member 4-hydroxybenzoyl-CoA thioesterase (subunits are colored dark teal) from *Arthrobacter* sp. strain AU (3) and YdiI from *E. coli* (subunits are colored gray). The bound ligands, 4-hydroxyphenacyl-CoA (black) and phenacyl-CoA (cyan), respectively are shown in stick. (C) Pymol stereo representation of the superposition of the tetrameric structures (dimer of dimers) of *E. coli* YbdB (cyan) and YdiI (gray) bound with phenacyl-CoA (shown in stick with cyan or gray carbon atoms, red oxygen atoms, blue nitrogen atoms, and yellow sulfur atoms). (D) Pymol representation of the of the tetrameric structure (dimer of dimer) of *E. coli* YdiI bound with phenacyl-CoA at the active site formed by subunits A, B, and C (shown in stick with green carbon atoms, red oxygen atoms, blue nitrogen atoms, and yellow sulfur atoms).

interpreted as evidence for an "under-evolved" enzyme (befitting the role of "scavenger"), it is now well recognized that substrate promiscuity is a key trait of highly evolvable enzymes (for review, see ref 13). We posit that this trait is inherent in the simplicity and plasticity of the architecture of the hotdog-fold.

Presently, we have carried out a case study of two paralogs, namely, YdiI and YbdB from *E. coli*. These thioesterases are related by 59% sequence identity and are distinguished by very diverse biological functions as detailed in the preceding companion paper[14] and depicted in Scheme 1. Briefly, in *E. coli*, YdiI participates in menaquinone biosynthesis as a catalyst for the hydrolysis of the pathway intermediate, 1,4-dihydroxynapthoyl-CoA.[14−16] YbdB, on the other hand, assists in the biosynthesis of the siderophore enterobactin through catalyzed hydrolysis of aberrant aroyl-*holo*EntB thioesters that, as dead-end pathway intermediates, act to block enterobactin formation.[17−19]

Herein, the structural determinants for substrate recognition and catalysis in these two paralogs are reported, and analyzed, within the context of evolution of hotdog-fold thioesterase function. In addition, because YdiI and YbdB are members of the same family clade as *Ar* 4-HB-CoA TE (Figure 1B and C),[3] a comparison of the relevant elements of structure and mechanism with those of this evolutionarily more distant relative is made, to identify those elements, which have been retained despite extensive sequence divergence. The findings are interpreted to suggest that a phosphopantethiene binding site is conserved for targeting CoA and *holo*ACP-based thioester metabolites, and that the location of the ACP or adenosine 3′,5′-diphosphate binding site on the surface of the thioesterase serves to promote promiscuity toward these two classes of thioesters. Furthermore, we infer that the divergence in the alkyl/aryl binding site sequence is important for the evolution of new biological function. Finally, we propose that the roles played by the conserved catalytic residues in thioester hydrolysis change in the process of adaptation of the thioesterase to its new physiological substrate.

MATERIALS AND METHODS

Materials. The substrate benzoyl-CoA was purchased from Aldrich/Sigma and the substrate 4-hydroxybenzyol-coenzyme A (4-HB-CoA) was synthesized as previously reported.[20] The inert substrate analog undecan-2-one-coenzyme A (UDO-CoA) was synthesized as reported in ref 12, and the inert substrate analogs 2,4-dihydroxyphenacyl-coenzyme A (2,4-DHP-CoA) and phenacyl-coenzyme A (P-CoA) were synthesized by reaction of CoA with 2-bromo-2′,4′-dihydroxyacetophenone or 2-bromo-acetophenone, respectively (see the Supporting Information for details). The enzymatic synthesis of [^{14}C]-benzoyl-CoA from [^{14}C]-benzoate, CoA, and ATP is detailed in the Supporting Information. Recombinant *E. coli* YbdB and YdiI, having C-terminal His_6-tags, were prepared as described in the companion paper.[14] Recombinant *E. coli* YbdB and YdiI, without the His_6-tags (i.e., native), were prepared as detailed in the Supporting Information.

Preparation of YbdB and YdiI Site-Directed Mutants. Site directed mutagenesis was carried out using the QuikChange PCR strategy (Stratagene) with the *ydiI-His*$_6$/pET-23a or *ybdB-His*$_6$/pET-23a plasmid as template and commercial primers and Pfu Turbo as the polymerase. The sequence of the mutated gene was confirmed by DNA sequencing. The recombinant plasmids were used to transform competent *E. coli* BL21 Star (DE3) cells. The mutant proteins were purified to >90% homogeneity (as determined by SDS-PAGE analysis), using the protocol described for the wild-type YdiI-His_6 and YbdB-His_6,[14] in a yield of 10−40 mg protein/g wet cell paste.

dx.doi.org/10.1021/bi500334v | *Biochemistry* 2014, 53, 4788−4805

Scheme 1. Biological Functions of *E. coli* YdiI and YbdB

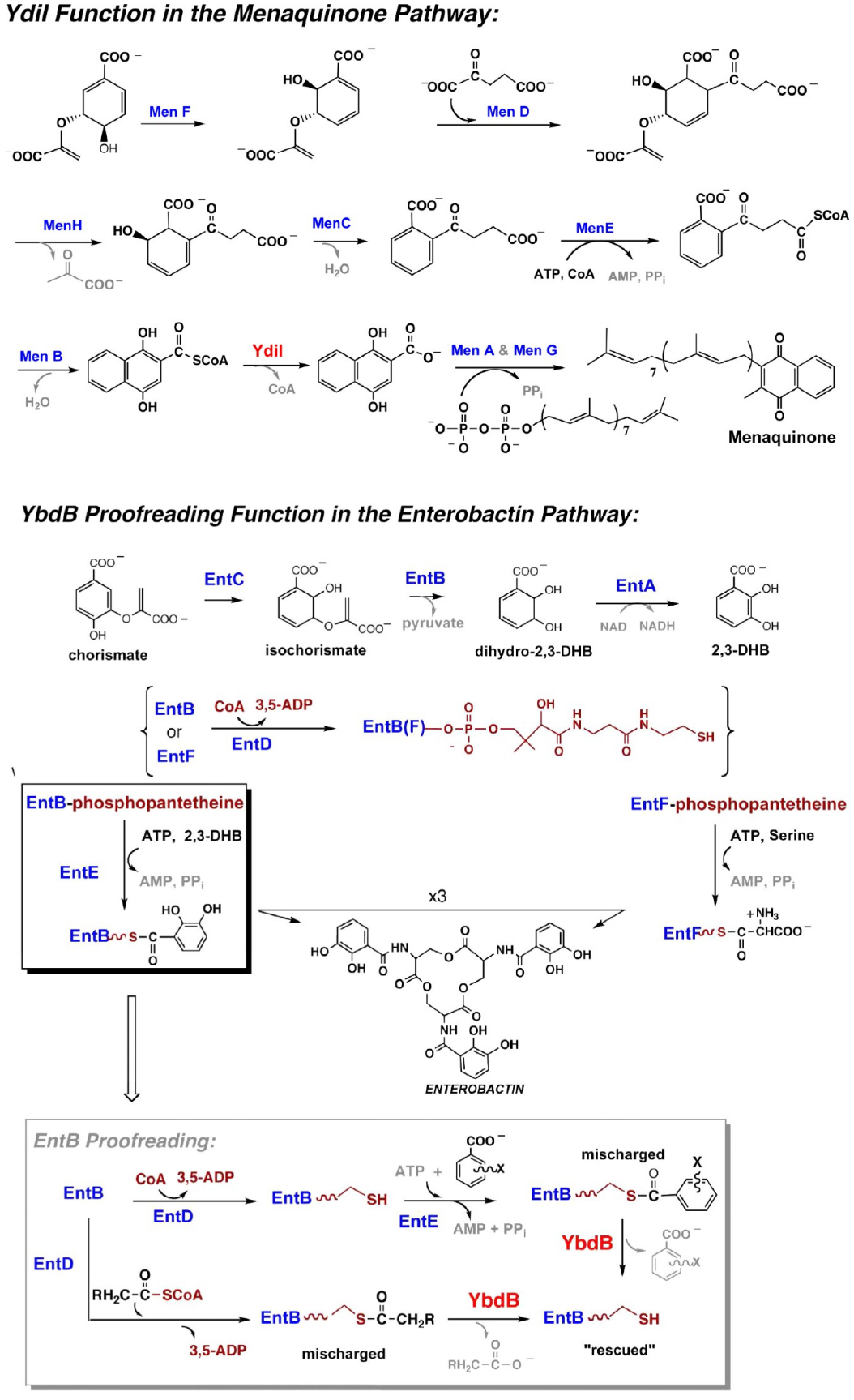

Determination of Steady-State Kinetic Constants. Thioesterase activity was measured using a 5,5′-dithio-bis(2-nitrobenzoic acid) (DTNB) coupled assay. Reactions were monitored at 412 nm ($\Delta\varepsilon$ = 13.6 $mM^{-1}\cdot cm^{-1}$) using a

dx.doi.org/10.1021/bi500334v | *Biochemistry* 2014, 53, 4788−4805

Beckman 640U spectrometer. Reactions were carried out at 25 °C in 0.5 mL solutions containing 50 mM K^+HEPES (pH 7.5), 1 mM DNTB, a known concentration of thioesterase, and varying concentrations of thioester ($0.5K_m$ to $5K_m$). The catalyzed hydrolysis of 4-HB-CoA in 50 mM K^+HEPES (pH 7.5) was directly monitored at 300 nm ($\Delta\varepsilon$ = 11.8 $mM^{-1}\cdot cm^{-1}$).

The initial velocity data, measured as a function of substrate concentration, were analyzed using the software program Enzyme Kinetics v1.4 and eq 1:

$$v = V_{max}[S]/([S] + K_m) \quad (1)$$

where v is the initial velocity, V_{max} is the maximum velocity, [S] is the substrate concentration, and K_m is the Michaelis constant. The k_{cat} was calculated from $V_{max}/[E]$, where [E] is the total enzyme concentration as determined by using the Bradford method.[21]

Inhibition constants (K_i) were determined by measuring the initial velocity at varying substrate concentration ($0.5K_m$ to $5K_m$) and fixed, changing inhibitor concentration (0, K_i, and $2K_i$). The data were fitted to eq 2 (to define the slope inhibition constant K_{is} for competitive inhibition) or to eq 3 (to define the respective intercept and slope inhibition constants K_{ii} and K_{is} for noncompetitive inhibition), respectively.

$$V = V_{max}[S]/[K_m(1+[I]/K_{is})+[S]] \quad (2)$$

$$V = V_{max}[S](1 + [I]/K_{ii})/[K_m(1+[I]/K_{is})+[S]] \quad (3)$$

where [I] is the inhibitor concentration, K_{is} is the slope inhibition constant, and K_{ii} is the intercept inhibition constant.

YdiI ^{18}O-Solvent-Labeling Experiments. A typical ^{18}O-labeling experiment was carried out as follows. A 4.0 mL solution containing 89 μM YdiI in 50 mM tris(hydroxymethyl)-aminomethane (Tris) and 50 mM NaCl (at pH 8.4) was lyophilized. To the resulting powder, 370 μL of 99.2% enriched $H_2{}^{18}O$ was added. After 15 min incubation on ice, the enzyme was assayed to confirm the retention of catalytic activity. To this solution, 30 μL of lyophilized (30 μL of 10 mM stock concentration in normal isotopic water) benzoyl-CoA suspended in 99.2% $H_2{}^{18}O$ water was added to yield final enzyme and substrate concentrations of 889 and 750 μM, respectively. The reaction mixture was incubated at room temperature for 15 min and then filtered using a 10 kDa microseparation filter (Millipore). The filtrate was acidified with 10 μL of 6 M HCl and extracted four times with 1 mL aliquots of ethyl acetate. The pooled extracts were dried over anhydrous sodium sulfate and the solvent was evaporated *in vacuo*. For the (multiple-turnover) control experiment, a 20 μL aliquot of the 89 μM YdiI stock solution was used. Following lyophilization, the resulting powder was suspended in 370 μL of 99.2% $H_2{}^{18}O$, and to this solution 30 μL of 10 mM benzoyl-CoA in 99.2% $H_2{}^{18}O$ was added. The final concentrations of YdiI and benzoyl-CoA were 45 and 750 μM, respectively. The GC/MS analyses were conducted using an Agilent 5975C Series GC/MS apparatus with a Triple-Axis detector. The temperature program used is as follows: 250 °C inlet, 80 °C initial temperature held for 1 min and ramped to 180 °C at a rate of 7 °C/min, then ramped to 250 °C at a rate of 20 °C/min and held for 6 min. The mass analyzer was set to detect in the range of 50−450 m/z. The benzoic acid eluted in the time frame of 7.5−8.0 min.

Rapid-Quench Studies of the YdiI-Catalyzed Hydrolysis of [^{14}C]benzoyl-CoA under Single and Multiple Turnover Conditions. Experiments were carried out at 25 °C using a rapid-quench instrument from KinTek Instruments. For the multiple-turnover reaction of YdiI-catalyzed hydrolysis of [^{14}C]-benzoyl-CoA, the final enzyme and substrate concentrations used were 10 and 50 μM, respectively, whereas for the single-turnover reaction, respective concentrations of 50 and 5 μM were employed. The reactions were initiated by mixing the enzyme with the [^{14}C]-benzoyl-CoA in 10 mM K^+HEPES buffer (pH 7.5) containing 0.1 M NaCl and then quenched after a specific time with 0.2 M HCl. The protein was separated from the quenched reaction mixture using a 10 000 MWCO centrifuge column (Millipore). The [^{14}C]-benzoyl-CoA and [^{14}C]-benzoic acid were separated on an analytical C18 column (RESTEK) by HPLC using the same procedures as described above, and then quantified using an in-line β-RAM4 (Lab Logic) scintillation counter. Peak integrations were performed by using Laura software (Lab Logic), and the relative ratios were used to calculate the substrate and product concentrations. The time course data were fitted by iterative simulation using the KinTek Corp. Global Kinetic Explorer software program.

YdiI Stopped-Flow Kinetic Experiments. A DX.17MV sequential stopped-flow spectrometer (Applied Photophysics, Leatherhead, U.K.) with a dead time of 3 ms was used for measurement of transient rate constants of YdiI-catalyzed hydrolysis of 4-HB-CoA. All reactions were carried out in triplicate using 50 mM K^+HEPES buffer (pH 7.5) at 25 °C as the solvent. The substrate concentration was monitored at 300 nm ($\Delta\varepsilon$ = 11.8 $mM^{-1}\cdot cm^{-1}$). A single-turnover reaction mixture initially consisted of 60 μL of 124 μM YdiI mixed with 60 μL of 100 μM 4-HB-CoA to give a final concentration of 62 μM YdiI and 50 μM 4-HB-CoA. The time course data were fitted to the single exponential eq 4. The multiple-turnover reactions contained 60 μL of 200 μM 4-HB-CoA mixed with 60 μL of 20, 32, and 40 μM YdiI. The final concentration of 4-HB-CoA was 100 μM, and the final concentrations of YdiI were 10, 16, and 20 μM.

$$Y_t = Y_0 + A\exp(-kt) \quad (4)$$

Y_0 and Y_t are the reaction solution absorbance at time t = 0 and t, respectively. A is the amplitude of the total absorbance change, and k is the apparent rate constant.

YbdB and YdiI Crystallization and X-ray Crystallographic Data Collection. Purified wild-type YbdB was concentrated to 10−15 mg/mL in 10 mM HEPES (pH 7.5), plus 0.15 M NaCl, 1 mM dithiothreitol (DTT), and purified wild-type YdiI was concentrated to 10 mg/mL in 20 mM Tris buffer pH 8.3, plus 50 mM NaCl. Initial crystallization conditions were identified using the Index Screen (Hampton Research) setup in Corning 96-well crystallography plates. Crystals of complexes of YbdB and YdiI with their respective inhibitors were obtained via cocrystallization of YbdB with 2,4-DHP-CoA or P-CoA or via cocrystallization of YdiI with 2,4-DHP-CoA, P-CoA, or UDO-CoA using the hanging-drop vapor diffusion method (0.5 mL well solution). In the case of YbdB, 1.0 μL of protein at 10−15 mg/mL was combined with well solution containing 2 mM substrate analog and 2.0 M sodium malonate (pH 7.0). In the case of YdiI, the drop volume, protein concentration, and substrate analog concentration were the same as those used for YbdB crystallization but the well solution contained 0.07−0.08 M sodium cacodylate (pH 6.5) and 0.18−0.20 M magnesium acetate. Crystals of YbdB·(2,4-DHP-CoA) and YbdB·(P-CoA) grew at 17 °C as

dx.doi.org/10.1021/bi500334v | *Biochemistry* 2014, 53, 4788−4805

Table 1. Crystallographic Data Collection and Refinement Statistics for *E. coli* YbdB and YdiI

subject	YdiI + 2,4-DHP-CoA	YdiI + P-CoA	YdiI + UDO-CoA	YbdB + 2,4-DHP-CoA	YbdB + P-CoA
PDB code	4K49	4K4A	4K4B	4K4D	4K4C
resolution (Å)[a]	43.14−1.89 (1.99−1.89)	44.61−1.97 (2.07−1.97)	35.80−1.80 (1.90−1.80)	50.0−2.17 (2.25−2.17)	50.0−1.85 (1.92−1.85)
space group	$P2_12_12$	$P2_12_12$	P1	$P2_12_12$	$P2_1$
unit cell (Å)	a = 97.9, b = 117.6, c = 48.0	a = 97.7, b = 117.9, c = 48.2	a = 58.0, b = 68.6, c = 81.1 α = 78.9, β = 84.7, γ = 76.5	a = 59.5,b = 85.9, c = 49.9	a = 51.4, b = 59.1, c = 85.9
R_{merge} [ab] (%)	8.2 (41.5)	6.2 (28.2)	8.8 (39.5)	9.3 (42.1)	5.7 (41.1)
completeness[a]	99.7 (98.2)	99.7 (97.9)	99.8 (99.7)	99.8 (100)	99.8 (100)
$I/I(\sigma)$[a]	11.8 (2.4)	18.5 (3.9)	14.2 (3.5)	11.1 (2.9)	13.7 (2.7)
redundancy[a]	7.7 (5.1)	12.6 (3.8)	8.2 (4.9)	9.9 (8.9)	3.7 (3.7)
total/unique reflections	45 005/6029	40 172/5340	110 184/16 443	141 246/14 280	164 296/44 184
R_{cryst}/R_{free} (%)	17.1/21.9	17.6/23.1	17.0/22.3	21.3/25.2	17.3/23.1
RMSD					
bond lengths (Å)	0.010	0.007	0.007	0.029	0.006
bond angles (deg)	1.359	1.117	1.100	2.006	1.032
average B-factors (Å^2)					
main chain	11.2	9.7	11.6	45.2	25.4
side chain	16.8	16.2	18.9	50.4	31.4
inhibitor	29.3	24.4	37.4[d]/50.8[e]	73.2[f]/168.0[g]	32.3[f]/95.2[g]
waters	28.6	26.5	33.1	49.1	37.5
Ramachandran plot					
core region (%)	98.3	98.1	98.5	96.3	97.4
allowed region (%)	1.7	1.9	1.5	3.7	1.9
outliers (%)	0	0	0	0	0.7

[a]Values for the highest resolution shell are given in parentheses. [b]$R_{merge} = \Sigma|I_i - I_m|/\Sigma I_i$, where I_i is the intensity of the measured reflection and I_m is the mean intensity of all symmetry-related reflections. [c]$R_{cryst} = \Sigma|F_{obs}| - |F_{calc}|/\Sigma|F_{obs}|$, where F_{obs} and F_{calc} are observed and calculated structure factors. $R_{free} = \Sigma|TF_{obs}| - |F_{calc}|/\Sigma|TF_{obs}|$, where T is a test data set of 5% of the total reflections randomly chosen and set aside prior to refinement. [d]Ligands bound to the active site [e]ligands bound on the protein surface [f]Average B-factor of pantetheine moiety [g]Average B-factor of nucleotide moiety

rectangular plates, to dimensions of ca. 0.2 × 0.2 × 0.05 mm^3 within 3 days. Crystals of YdiI·(2,4-DHP-CoA), YdiI·(P-CoA), and YdiI·(UDO-CoA) grew at 17 °C to the dimensions of 0.2 × 0.2 × 0.1 mm^3 within 4 days.

YbdB·(2,4-DHP-CoA) crystals were transferred to paratone N and flash-cooled in a stream of gaseous N_2 at 100 K, whereas YbdB·(P-CoA) crystals were directly frozen in liquid nitrogen without additional cryoprotection. YdiI·(2,4-DHP-CoA), YdiI·(P-CoA), and YdiI·(UDO-CoA) crystals were dehydrated by soaking for 5 min in paratone N before flash-cooling in a stream of gaseous N_2 at 100 K. X-ray diffraction data for crystalline YbdB·(P-CoA) were collected at the National Synchrotron Light Source, Brookhaven National Laboratory, Beamline X12C and then processed using HKL2000.[22] X-ray diffraction data for crystalline YbdB·(2,4-DHP-CoA) were collected using Cu Kα radiation from a Rigaku RU-300 generator equipped with an R-Axis IV++ image plate (Boston University School of Medicine) and then processed using DENZO and SCALEPACK.[22] All other data sets were collected on a Bruker MICROSTAR microfocus rotating anode with Helios optics equipped with a Platinum 135 CCD detector using a four-circle kappa goniometer (Boston University) and then processed using Bruker Proteum 2 software. The data collection and processing statistics are provided in Table 1.

Refinement of the X-ray Structures of YbdB and YdiI Bound with Substrate Analogs. Phases for all structures were determined by molecular replacement using the known structures of *apo*-YbdB (PDB ID 1VH9; ref 24) and *apo*-YdiI (PDB ID 1SBK; Northeast Structural Genomics Consortium), as the respective search models, in conjunction with the MOLREP software of the CCP4 program package.[23] The models thus generated were refined with PHENIX[25] using individual B-factor refinement (occupancies were not refined). Waters were added using Coot's water picking algorithm and then were manually inspected to ensure good placement.[26] The final models were validated using tools implemented in PROCHECK.[27] The dihedral angles of all residues are within the allowed region of the Ramachandran plot. Refinement statistics and model geometry for all five structures are listed in Table 1. The final model of the YbdB·(2,4-DHP-CoA) complex includes two YbdB subunits and two 2,4-DHP-CoA molecules minus the C-terminal Gly137 in both subunits, and the Leu136 in subunit B. The final model of the YbdB·(P-CoA) complex includes four YbdB subunits (two dimers) and four P-CoA

dx.doi.org/10.1021/bi500334v | *Biochemistry* 2014, 53, 4788−4805

molecules. The final models of the YdiI complexes include four subunits and four 2,4-DHP-CoA or P-CoA ligands, plus eight subunits with 13 UDO-CoA molecules (eight are bound to the active sites and five are located at the protein surface). The refinement statistics are summarized in Table 1.

RESULTS AND DISCUSSION

Structural Determinants of YbdB and YdiI Substrate Specificity and Catalysis. For the purpose of examining the structural determinants for substrate binding, 2,4-dihydroxyphenacyl-CoA (2,4-DHP-CoA), phenacyl-CoA (P-CoA), and undecan-2-one-CoA (UDO-CoA) (see Chart 1 for chemical structures) were synthesized to serve as stable keto-thioether (O=C−CH_2—S) analogs of the corresponding *in vitro* thioester substrates 2,4-dihydroxybenzoyl-CoA, benzoyl-CoA, and decanoyl-CoA, respectively.[14] The K_{is} values, determined for the analogs as competitive inhibitors of YbdB and YdiI-catalyzed benzoyl-CoA hydrolysis are reported in Table 2 (the Lineweaver−Burk plots are shown in Figure SI1 in the Supporting Information). The structures of YbdB in complex with 2,4-DHP or P-CoA were determined,[c] as were structures of the respective YdiI complexes derived from all three substrate analogs (the statistics are reported in Table 1; the electron density maps of the bound ligands are shown Figure SI2 in the Supporting Information).

Chart 1. Structures of Selected Substrates, Substrate Analogs, and Products: 1,4-Dihydroxynapthoyl-CoA (1), 2-Hydroxybenzoyl-*holo*EntB (2), Benzoyl-CoA (3), Coenzyme A (4), 2,4-Dihydroxyphenacyl-CoA (5), and Undecan-2-one-CoA (6)

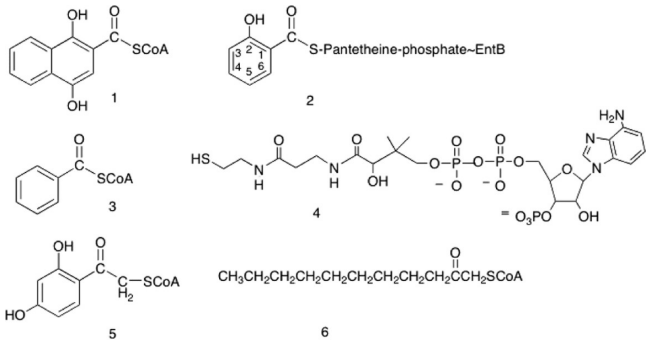

Table 2. Steady-State Competitive Inhibition Constants (K_{is}) for Substrate Analog and Product Inhibitors of YbdB- or YdiI-Catalyzed Hydrolysis of Benzoyl-CoA (or 4-Hydroxybenzoyl-CoA) at pH 7.5 and 25 °C[a]

	K_{is} (μM)	
inhibitor	YbdB	YdiI
phenacyl-CoA	65 ± 6	7.8 ± 0.4
2,4-DHP-CoA	5.9 ± 6	2.5 ± 0.2
DUO-CoA		12.2 ± 0.5
CoA[b]	210 ± 10[c]	16 ± 1

[a]See Materials and Methods for details. [b]The substrate used was 4-hydroxybenzoyl-CoA, and the reaction was monitored at 300 nM. [c]Noncompetitive inhibition was observed: K_{is} = 210 ± 10 μM and K_{ii} = 1130 ± 100 μM.

The YbdB (137 amino acids) and YdiI (136 amino acids) quaternary structures are best described as a dimer of dimers (see superimposed structures in Figure 1C and the YdiI structure, with subunits labeled, in Figure 1D). The monomer possesses a five-turn α-helix, which is wrapped by a sheet formed by five antiparallel β-strands. Monomers associate in the usual manner, β-sheet-edge-to-β-sheet-edge, to form an elongated sheet, which stacks back-to-back with the sheet of the opposing dimer; the four respective central α-helices are thus located at the solvent interface. Both the tertiary and quaternary structures of YbdB and YdiI thioesterases are closely matched, and they are quite similar to those of the prototype of the type AB clade, 4-hydroxybenzoyl-CoA thioesterase from *Arthrobacter* sp. strain AU (*Ar* 4-HB-CoA TE)[3] (Figure 1B).

The four YdiI or YbdB active sites are located at the interfaces of the subunits that comprise the respective dimer units. A loop from one of the two subunits of the opposing dimer appears to contribute to ligand binding through interaction with the ligand pyrophosphate moiety. Henceforth, the subunits which form paired active sites are referred to as subunits "A" and "B", and the subunit that contributes the pyrophosphate-binding loop as subunit "C" (for illustration, see YdiI in Figure 1D). In the text and figures that follow, the residues located on designated subunit C are labeled with a double asterisk (**), those located on subunit B with a single asterisk (*), and those located on subunit A are not labeled with an asterisk.

The structures of the respective YbdB·(2,4-DHP-CoA) and YbdB·(P-CoA) complexes superimpose with the structure of the *apo*-YbdB structure (PDB 1VH9) with Cα RMSD values of 0.37 and 0.43 Å, respectively. Likewise, the structures of the YdiI·(2,4-DHP-CoA) and YdiI·(P-CoA) complexes superimpose with the structure of *apo*-YdiI (PDB entry 1SBK) with Cα RMSD values of 0.58 and 0.56 Å, respectively. Only in the case of the structure of the YdiI·(UDO-CoA) complex are significant ligand-induced conformational changes observed (RMSD 1.14−1.18 Å). Three secondary structural elements (α-helix residues Leu9-Gly16 and loop residues Gln48-Leu53 and Thr74-Lys79; Figure SI3 in the Supporting Information), located at the acyl-binding site region of the active site, shift to expand the binding pocket occupied by the long UDO-CoA aliphatic chain (Figure 2A). In contrast, the binding pockets observed in the YdiI·(P-CoA) (Figure 2B) and YbdB·(P-CoA) (Figure 2C) are unchanged.

Overall, the three-dimensional structures of YbdB and YdiI are highly similar despite the noted divergence in sequence. The pairwise sequence alignment and the locations of substituted residues on the three-dimensional structure are provided in the Supporting Information (Figure SI4). Here, we examine the differences in YbdB and YdiI active site residues and their interaction with the different substrate analogs. For convenience, the findings are presented by section starting with the binding interactions involving the substrate CoA nucleotide, followed by the phosphopantetheine arm, the thioester substituent, and, last, the aryl or alkyl unit.

Structure analysis and Mutagenesis of the CoA Nucleotide-Binding Site. The substrate specificity profile analysis reported in the companion paper[14] showed that YdiI and YbdB are highly active catalysts toward the hydrolysis of thioesters containing CoA as the thiol group. For instance, the substrate specificity constants (k_{cat}/K_m) measured for the YdiI- and YbdB-catalyzed hydrolysis reactions of benzoyl-CoA are 7 × 10^5 and 2 × 10^5 $M^{-1}·s^{-1}$, respectively (Table 3). The X-ray

dx.doi.org/10.1021/bi500334v | *Biochemistry* 2014, 53, 4788−4805

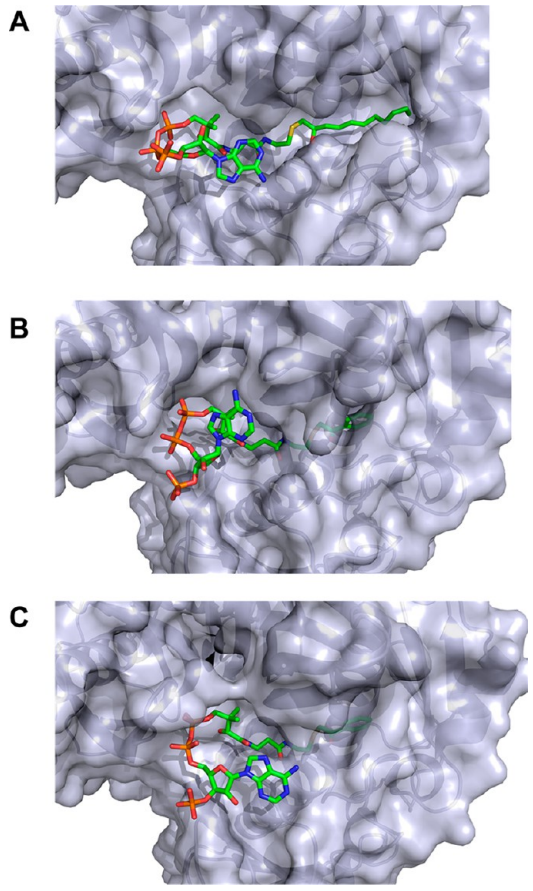

Figure 2. Pymol (surface) representations of the solvent accessibility of the bound ligands of the (A) YdiI·(undecan-2-one-CoA), (B) YdiI·(phenacyl-CoA), and (C) YbdB·(phenacyl-CoA) complexes. The ligands are shown in stick with green carbon atoms, red oxygen atoms, blue nitrogen atoms, orange phosphorus atoms, and a yellow sulfur atom.

Table 3. Steady-State Kinetic Constants for Wild-Type and Mutant YdiI- and YbdB-Catalyzed Hydrolysis of Benzoyl-CoA Measured at pH 7.5 and 25 °C

YdiI	k_{cat} (s^{-1})	K_m (μM)	k_{cat}/K_m ($\mu M^{-1}\cdot s^{-1}$)
wild-type	17.7 ± 0.7	25 ± 3	7.2×10^5
E63A	$<1 \times 10^{-4}$		
E63Q	$<1 \times 10^{-4}$		
E63D	0.040 ± 0.002	120 ± 10	3.4×10^2
Q48A	0.051 ± 0.002	12 ± 1	4.4×10^2
Q48N	0.18 ± 0.01	12.6 ± 0.8	1.4×10^4
S67A	2.5 ± 0.1	12.6 ± 0.2	2.0×10^5
S64A	1.7 ± 0.1	11.9 ± 0.9	1.4×10^5
H89A	0.82 ± 0.02	180 ± 10	4.6×10^3
H54A	0.14 ± 0.01	100 ± 8	1.4×10^3
H54F	0.015 ± 0.001	16.8 ± 0.9	8.9×10^2
H106A	16.9 ± 0.1	41 ± 2	4.1×10^5
R91A	1.9 ± 0.4	23 ± 3	8.2×10^4
S109A	8.1 ± 0.4	14.2 ± 0.2	5.8×10^5
YbdB	k_{cat} (s^{-1})	K_m (μM)	k_{cat}/K_m ($\mu M^{-1}\cdot s^{-1}$)
wild-type	2.2 ± 0.1	12 ± 1	1.8×10^5
E63A	$<1 \times 10^{-4}$		
Q48A	$<1 \times 10^{-4}$		
H54A	$<1 \times 10^{-4}$		
M68V	1.8 ± 0.1	24 ± 2	7.5×10^4

structures of the YbdB and YdiI complexes indicate that the CoA nucleotide-binding site is formed at the interface of subunits A−C (Figure 3A). The nucleotide moiety resides at the protein surface where it interacts with surface residues via the 3′-phosphate (hydrogen bond formation with the Arg91 side chain) and 5′-pyrophosphate (hydrogen bond formation with the backbone amide NHs of the hairpin turn residues 109**, and 110**, and 111**) (Figure 3B). The high B-factors (Figure SI5, Supporting Information) observed for the atoms of the nucleotide compared to the surrounding protein side-chains in the crystalline complex indicate motion or disorder and thus, the absence of tight binding (note that the occupancies were not refined). The polar side chains of the β-turn-β motif of subunit C could conceivably interact with the nucleotide if they were to assume alternate, yet accessible, rotomer conformations. However, aside from His106**, these residues differ between YbdB and YdiI (Figure 3B; sequence alignment shown in Figure SI4A in the Supporting Information), and furthermore, they are not stringently conserved among the respective sets of YbdB and YdiI orthologs.[14] The differences in the residues that frame the nucleotide binding sites in YdiI and YbdB culminate in the formation of two very distinct surface topologies having unique steric and electrostatic features (Figure 3C).

Ala mutants were constructed to independently query if the side chains of the stringently conserved residues Arg91 and His106** contribute to substrate binding. At the same time, the Ala mutant was made to test the contribution by side chain of Ser109**, which in the YdiI structure is located within hydrogen bond distance of the 5′-α-phosphate group (Figure 3B). The steady-state kinetic constants k_{cat} and k_{cat}/K_m were determined for hydrolysis of the benzoyl-CoA substrate, catalyzed by the purified mutant enzymes (Table 3). The k_{cat} and k_{cat}/K_m values measured for S109A** and H106A** YdiI are not significantly different from those measured for wild-type YdiI. On the other hand, the k_{cat} and k_{cat}/K_m values measured for the R91*A YdiI is reduced ∼10-fold, indicating that Arg91* facilitates productive (i.e., oriented for catalysis) substrate binding. We note here, and will revisit in later discussion, that Arg91* corresponds to Arg102* in clade AB prototype *Ar* 4-HB-CoA TE, wherein Arg102* has been shown to contribute to substrate binding.[3,28]

Structure of the Pantetheine-Binding Site. The pantetheine arm assumes an extended conformation as it threads through the tunnel-like channel formed by residues His89, His90 (Val90 YdiI), Arg91, Pro92 (Ser92 YdiI), Gly55, and Leu52 located on one subunit and by the residues Gly82* and Val81* located on the opposing subunit (Figure 4A). The backbone amide C═Os of His(Val)90 and Gly82* are positioned to form hydrogen bonds with the respective NH functions of the pantetheine moiety. The side chains of Pro(Ser)92, Leu52, and Val81* enclose the binding site, excluding solvent. The B-factors of the atoms that comprise the pantetheine arm are similar to those of the surrounding side chains (∼7−12 Å^2) indicating that these are the most highly immobilized atoms of the ligand in its bound state (Figure SI5, Supporting Information).

The hydrogen bond formation, combined with the desolvation of the hydrophobic sites, and the van der Waals attractive forces acting on the closely packed atoms are expected to generate substantial binding energy. Indeed, the binding energy derived from the pantetheine arm, combined with the small contribution made by the weak protein surface interactions with the nucleotide, leads to tight CoA binding (Table 2) and,

dx.doi.org/10.1021/bi500334v | *Biochemistry* 2014, 53, 4788−4805

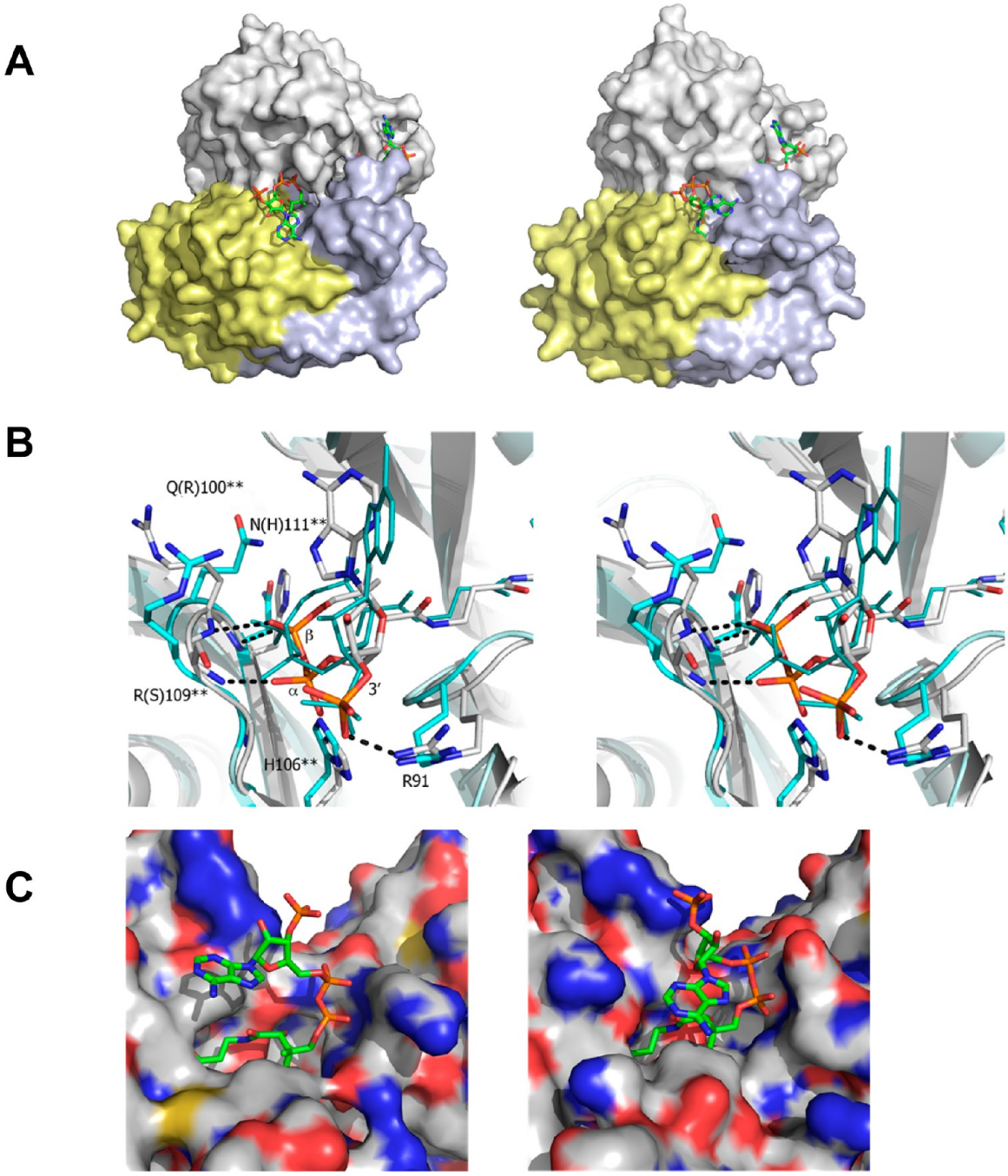

Figure 3. (A) YbdB·(P-CoA) (left) and YdiI·(P-CoA) (right) complexes with the subunit A colored white-blue, subunit B yellow, and subunit C gray. The P-CoA ligands are shown in stick using the same coloring scheme used in Figure 2 (B). Stereo figure made in Pymol showing the comparison of the CoA nucleotide binding sites of the superimposed structures of the YbdB·(P-CoA) (pale cyan backbone, cyan side chain carbon atoms, and teal ligand carbon atoms) and YdiI·(P-CoA) (gray) complexes. The dashed lines represent the hydrogen bonds made between the P-CoA pyrophosphate group and the backbone amide NHs of the YdiI subunit C hairpin loop. (C) Protein surface at the CoA nucleotide-binding site observed in the YbdB·(P-CoA) (left) and YdiI·(P-CoA) (right) complexes.

hence, to tight substrate binding. In addition, the steric and electrostatic properties of the binding site are likely to play a key role in the placement of the thioester moiety in register with the catalytic residues, as required for productive substrate binding, a determinant of turnover rate (k_{cat}).

Structure Analysis and Mutagenesis of the Catalytic Site. The substrate thioester group and the YdiI/YbdB active site residues that surround it comprise the reaction center. The structures of YdiI and YbdB bound with P-CoA represented in Figure 4B show that the residues at this site are conserved, and that the positions of the respective P-CoA ligands are the same (Figure 4B). However, to the extent that the steric properties of the inhibitor methlyene ketone moiety (O═C—CH_2SCoA) differ from those of the substrate thioester moiety (O═C—SCoA), the observed alignment of the catalytic residues is an approximation. Nevertheless, we find that the P-CoA ring carbonyl group is positioned to accept a hydrogen bond from the α-helix Gly55 backbone amide NH moiety, and to interact with the positive pole of the helix macro dipole. Substrate activation via polarization of the thioester C═O by the α-helix

dx.doi.org/10.1021/bi500334v | *Biochemistry* 2014, 53, 4788−4805

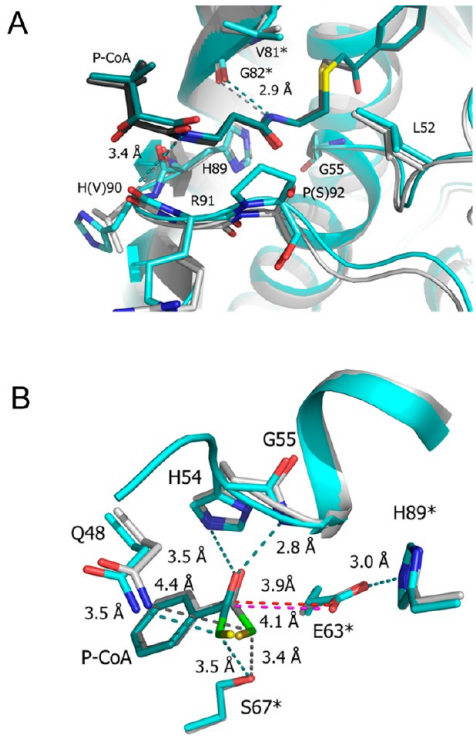

Figure 4. Superposition of the structures of the YbdB·(P-CoA) and YdiI·(P-CoA) complexes (enzyme carbon atoms are colored cyan and gray, respectively; ligand carbons atoms colored teal and dark gray, respectively). The distances (Å) between potential hydrogen bond donors and acceptors are shown for YdiI (dark gray) and YbdB (teal). The side chains are shown in stick and labeled to identify the conserved residue, or with the YbdB residue followed by YdiI residue in brackets. (A) Pantetheine moiety binding site is shown. (B) Catalytic site is shown. The red and magenta colored dashed-lines connect the phenacyl carbonyl carbon atom with the one of the two Glu63* carboxylate group oxygen atoms.

N-terminus is common to the catalytic mechanisms employed by hotdog-fold thioesterases.[2,3,28−32] It is therefore a component of the posited catalytic mechanism(s) depicted in Scheme 2.

The YbdB and YdiI reaction centers also include His54, Gln58, and Ser67*. The imidazole ring N(1) of His54 is located in close proximity to the P-CoA O═C—CH_2 oxygen atom; however, the orientation of the imidazole ring observed in the structure is not consistent with hydrogen bond formation with the ligand C═O (Figure 4B). We speculate that the stringent conservation of His54 is the result of the space-filling property of its imidazole ring, which might contribute to the alignment of neighboring residues. Notably, the replacement of the His54 residue with Ala resulted in a 126-fold reduction in k_{cat} and a 514-fold reduction in k_{cat}/K_m as measured for H54A YdiI-catalyzed benzoyl-CoA hydrolysis (Table 3). The H54A YbdB mutant proved to be inactive. Thus, His54 appears to be an important residue for catalysis.

The methylene carbon atom (highlighted green in Figure 4B) of the P-CoA O═C—CH_2 moiety corresponds to the substrate thioester sulfur atom. In the YbdB structure, the methylene carbon atom is within close proximity of the Gln48 side chain NH_2 and the Ser67* side chain OH, which indicates possible substrate activation via hydrogen formation with one or both hydrogen bond donors. On the other hand, in the YdiI structure, the methylene carbon atom of the P-CoA O═C—CH_2 moiety is more distant from the Gln48 NH_2, but it is still in close proximity of the Ser67* hydroxyl group. To assess whether Gln48 and Ser67* are required for efficient catalysis, the respective Ala mutants were prepared for steady-state kinetic analysis. Compared to the kinetic constants measured for benzoyl-CoA hydrolysis catalyzed by wild-type YdiI, the Q48A YdiI mutant k_{cat} value was reduced 354-fold and the k_{cat}/K_m value was reduced 1800-fold (Table 3). The Q48A YbdB mutant was found to be inactive. Therefore, we conclude that Gln48 plays an important role in YdiI and YbdB catalysis, and thus, in Scheme 2 we depict hydrogen bond formation between Gln48 and the CoA thiolate-anion leaving group. On the other hand, Ala replacement of YdiI Ser67* reduced the k_{cat} value only 7-fold and the k_{cat}/K_m value only 4-fold (Table 3) (YbdB was not tested). This finding indicates that Ser67* does not make a major contribution to catalytic efficiency.

The side chains of stringently conserved His89* and Glu63* are aligned for formation of a hydrogen bond between the N(3)H (of the corresponding imidazole tautomer) and one of the two Glu63* carboxylate oxygen atoms (Figure 4B, Scheme 2). This interaction orients the Glu63* carboxylate group and thus, it is expected to assist Glu63* as the active site nucleophile, or base catalyst. Ala replacement of the YdiI His89* residue results in a 22-fold reduction in k_{cat} and a 288-fold reduction in k_{cat}/K_m as measured for catalyzed benzoyl-CoA hydrolysis (Table 3). Catalytic activity could not be detected for the E63*A and E63*Q YdiI mutants, nor was it observed for the E63*A YbdB mutant. The E63*D YdiI mutant was found to retain some activity; however, the k_{cat} is reduced 443-fold and the k_{cat}/K_m is reduced 2118-fold relative to the corresponding wild-type YdiI kinetic constants (Table 3). We conclude that the carboxylate group of the Glu63* residue and the length of the Glu63* side chain are critical determinants of catalysis. The His89* contributes to the catalytic efficiency through the assisted alignment of Glu63*.

The close proximity of the Glu63* carboxylate group to the P-CoA O═C—CH_2 carbonyl carbon (Figure 4B), observed in the YdiI and YbdB complexes is consistent with the role of Glu63* as the catalytic base or nucleophile (Scheme 2). Unfortunately, the orientation of the Glu63* carboxylate group observed in the respective structures does not allow the distinction to be made between Glu63* function in nucleophilic catalysis and Glu63* function in base catalysis. First, the O═C—CH_2 moiety is not properly aligned with the Glu63* carboxylate group for nucleophilic attack,[33] and second, there is insufficient space between the carbonyl carbon and the Glu63* carboxylate group for a water molecule to bind (see Figure SI6 in the Supporting Information). Owing to this ambiguity, we were impelled to carry out further investigation, namely, the ^{18}O-solvent isotope labeling and transient kinetic studies reported below.

Structure of the Aryl/Alkyl Group-Binding Site. The alky/aryl group-binding sites of YdiI and YbdB are located at the subunit−subunit interfaces formed within the respective dimer units (Figure 5A). The structures of YbdB and YdiI bound with P-CoA reveal a solvent inaccessible aryl group-binding site in the case of YbdB (Figure 2C), and a partially open aryl group-binding site in the case of YdiI (Figure 2B). The substrate aryl/alkyl group-binding regions in YdiI and YbdB are largely conserved (Figure 5B). The common residues include Val80, Val81, His54, Pro49, Phe50, Gln48, and Glu63* plus Ser67*, whereas binding site residues Phe71*, Met68*, and Thr15* of the YbdB correspond to the YdiI residues Tyr71*, Val68*, and

dx.doi.org/10.1021/bi500334v | *Biochemistry* 2014, 53, 4788−4805

Scheme 2. Two Chemical Pathways for YdiI- and YbdB-Catalyzed Hydrolysis of Benzoyl-CoA and the Roles That the Amino Acid Residues at the Respective Catalytic Sites Might Play in Catalysis[ad]

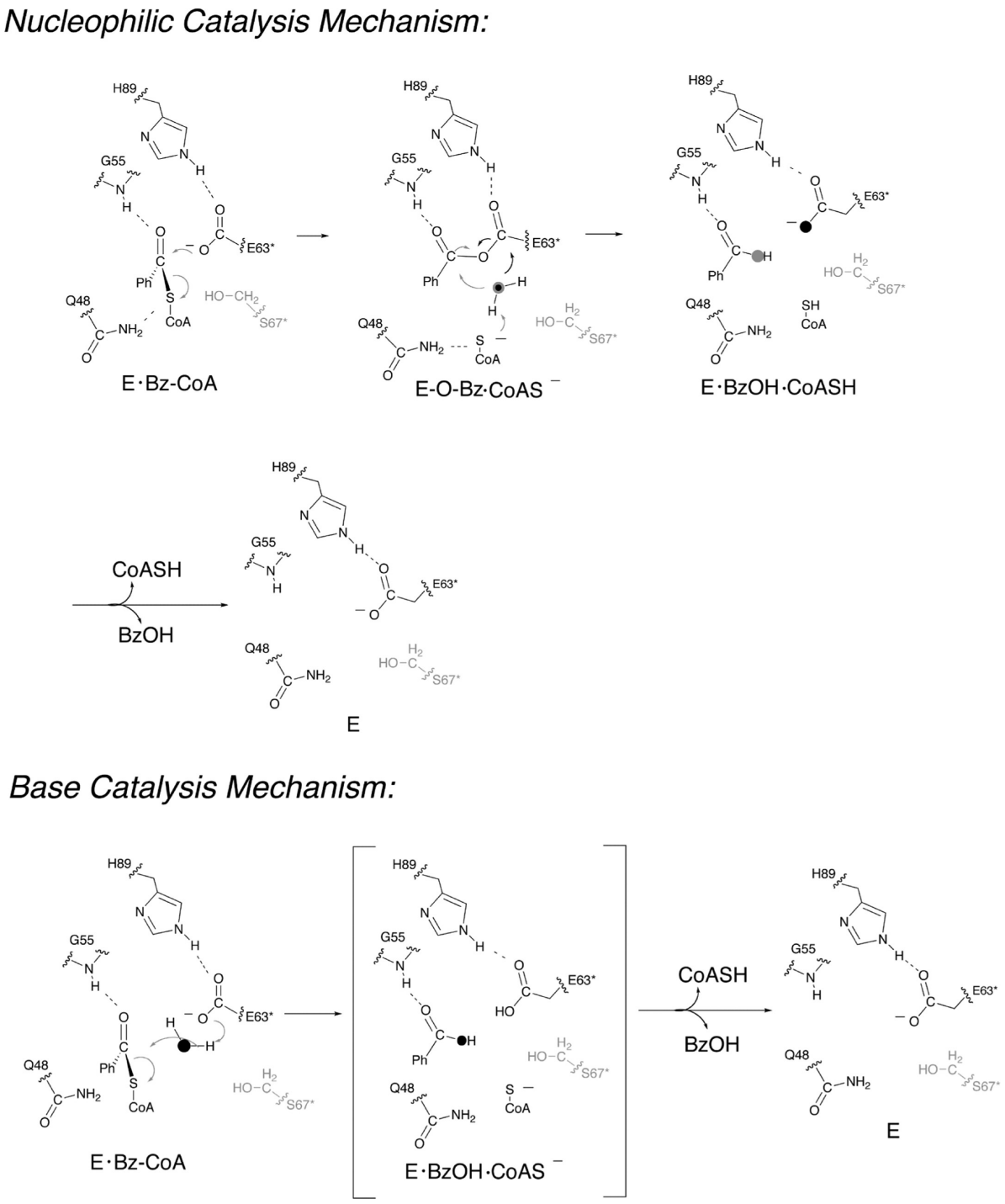

[a]The oxygen atom transfer from water to Glu63* (black filled circle) or benzoic acid (gray filled circle) is illustrated.

Met15*. The aromatic rings of the conserved Phe50 residues and of the YdiI Tyr71* and YbdB Phe71* residues contribute to solvent exclusion (Figure 5A and B and Figure SI3 in the Supporting Information).

The comparatively high catalytic efficiencies that YbdB and YdiI display with benzoyl-CoA serving as substrate, suggests that the benzoyl groups of the respective physiological substrates (hydroxy)benzoyl-*holo*EntB and 1,4-dihydroxynaphthoyl-CoA serve as the key substrate recognition motif. Indeed, the findings from the substrate specificity analysis demonstrated that ring hydroxylation does not significantly alter the value of k_{cat}/K_m.[14] To gain insight into the mode of interaction between the binding pocket and the hydroxylated benzoyl ring, the X-ray crystal structures of YbdB and YdiI in complex with 2,4-DHP-CoA were determined. As shown in Figure 5C, the O═C—CH_2S groups of the 2,4-DHP-CoA ligands are similarly oriented through hydrogen bond formation with the Gly55 backbone amide NH. On the other hand, the 2,4-dihydrox-

dx.doi.org/10.1021/bi500334v | *Biochemistry* 2014, 53, 4788−4805

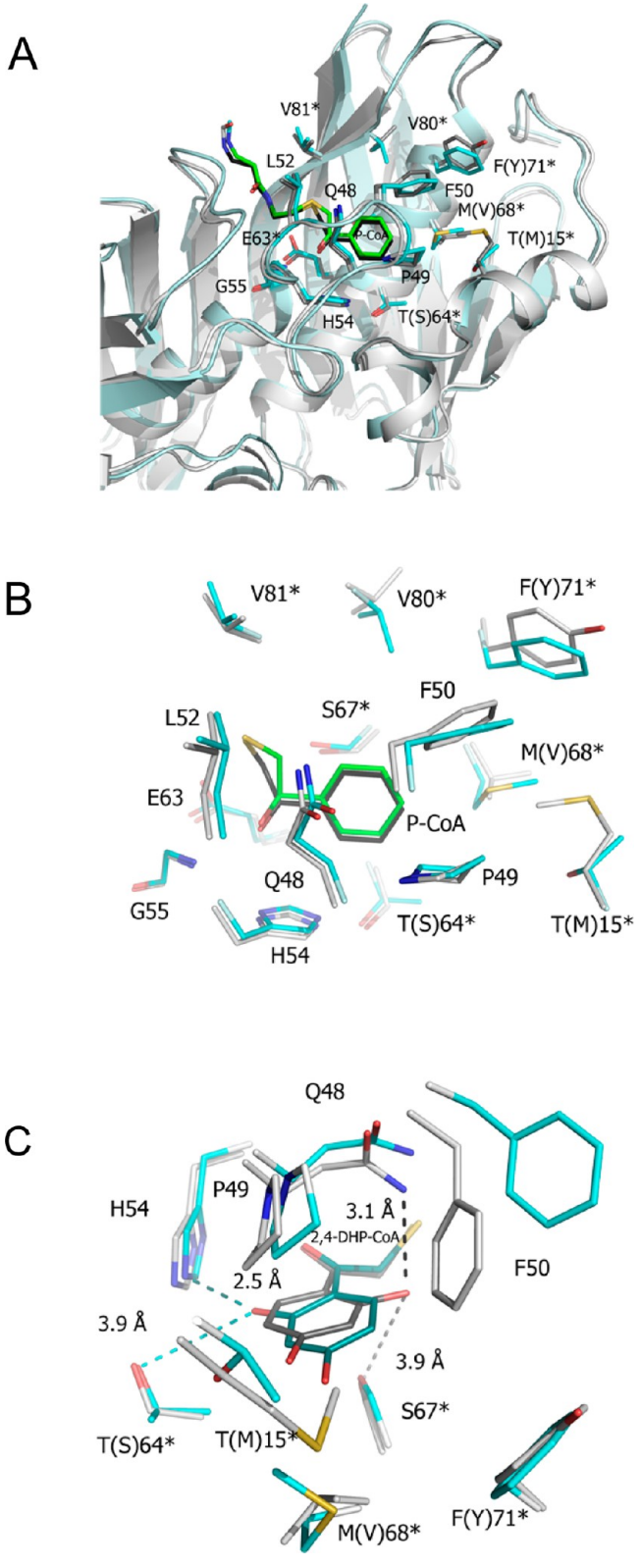

Figure 5. (A, B) Superposition of the structures of the YbdB·(phenacyl-CoA) and YdiI·(phenacyl-CoA) complexes (enzyme carbon atoms are colored cyan and gray, respectively; ligand carbons atoms colored green and black, respectively) to show the residues that contribute to the phenacyl binding pocket in the context of the residues that form the catalytic site. Panel (A) shows the locations of the residues on the main chain of subunit A and of subunit B, whereas panel (B) highlights the residues. (C) Superposition of the structures of the YbdB·(2,4-dihydroxyphenylacyl-CoA) and YdiI·(2,4-dihydroxy-

Figure 5. continued

phenacyl-CoA) complexes (enzyme carbon atoms colored cyan and gray, respectively; ligand carbons atoms colored teal and gray, respectively) to show the residues that form hydrogen bonds with the ring hydroxyl groups (dashed lines colored teal or black for the short bond distances and gray and cyan for the long bond distances; lengths are shown in angstroms).

yphenyl rings are "flipped" 180° relative to one another. The ring orientation observed in YbdB allows hydrogen bond formation between the ring C(2)OH and the His54, whereas the ring orientation observed in YdiI allows hydrogen bond formation between the ring C(2)OH and the Asn48.

Kinetics and Mechanisms of YdiI Catalysis. *Glu63* Function in Catalysis.* The X-ray crystallographic structures of YdiI and YbdB bound with inhibitors, and the kinetic properties of the respective Glu63* site-directed mutant enzymes, support Glu63* as the key catalytic residue. However, as noted previously, the structural data do not allow a clear distinction to be made between the role of Glu63* in catalysis as the nucleophile or the general base (Scheme 2). With the objective of making this distinction, we carried out transient kinetic and solvent ^{18}O-labeling experiments. Precedent for the experimental approach employed here derives from earlier work performed on the type AB and type AA clade prototypes,[a] *Ar* and *Ps* 4-HB-CoA TE. For both thioesterases, catalysis proceeds via the nucleophilic catalysis pathway with rate-limiting hydrolysis of the mixed anhydride intermediate formed with the Asp17 of *Ps* 4-HB-CoA TE or with the Glu73* of *Ar* 4-HB-CoA TE.[28,31]

To provide context for the experimental results reported below, we first point out that the time courses measured for the *Ps* and *Ar* 4-HB-CoA thioesterases defined a rapid "burst" of substrate consumption associated with the first catalytic turnover of 4-HB-CoA followed by a slower steady-state rate followed in subsequent turnovers. These results, combined with the observation of normal solvent kinetic isotope effects on the respective k_{cat} values, were interpreted as evidence for the formation of the mixed anhydride intermediate in the catalytic pathways of these thioesterases. Second, we note that the solvent ^{18}O-labeling experiments that were carried out to determine the regiochemistry of hydrolytic cleavage of the mixed anhydride intermediate formed from 4-HB-CoA showed that with the *Ps* 4-HB-CoA TE intermediate hydrolysis occurred solely at the 4-hydroxybenzoyl carbonyl carbon,[31] whereas with the *Ar* 4-HB-CoA TE intermediate hydrolysis occurred with 90% $H_2{}^{18}O$ attack at the 4-hydroxybenzoyl carbonyl carbon and 10% at the Glu73* carbonyl carbon.[28] Finally, we showed (1) that the burst phase kinetics and the 10% transfer of ^{16}O from enzyme to the 4-hydroxybenzoate product are not displayed by the *Ar* 4-HB-CoA TE E73D* mutant, consistent with a switch from nucleophilic catalysis to base catalysis, and (2) that the *Ar* 4-HB-CoA TE T77A* mutant displays burst phase kinetics, a 10-fold reduction in the rate constant governing the hydrolysis of the mixed anhydride intermediate, and the loss of regiospecifity in $H_2{}^{18}O$ attack[28] (consistent with the role of Thr77* in orienting the water nucleophile for attack at the 4-hydroxybenzoyl carbonyl carbon).

The Presteady-State Time Course for YdiI Catalysis. Because YdiI proved to be the more robust of the two paralogs, it was used as the experimental subject. Transient

dx.doi.org/10.1021/bi500334v | *Biochemistry* 2014, 53, 4788−4805

kinetic methods were employed to monitor substrate consumption over the first few catalytic turnovers to detect nucleophilic catalysis by observing a "burst phase" (for formation of the reaction intermediate) associated with the first turnover. Accordingly, stopped-flow absorbance techniques were used to measure the time course for the initial turnovers of 4-HB-CoA, catalyzed by YdiI, at pH 7.5. The 4-HB-CoA was employed as substrate because the *para*-hydroxybenzoyl-thioester chromophore possesses a strong absorption band at 300 nm, which is eliminated upon cleavage of the thioester substituent. Thus, the progress of the reaction could be monitored directly, that is, without the use of the DTNB coupling agent.

Note that if the rate of thioester cleavage is fast relative to an ensuing step (e.g., the hydrolysis of the mixed anhydride intermediate formed by Glu63*), the rate of the first catalytic turnover will exceed the rate of subsequent turnovers. In addition, if the internal equilibrium position favors the forward direction, the amount of substrate consumed will roughly correspond to the concentration of the YdiI employed in the reaction, which is set at a level high enough for monitoring a single turnover. The predicted "burst" of substrate consumption was, however, not observed in the time courses measured for the hydrolysis of 100 μM 4-HB-CoA in the presence of 10, 16, or 20 μM YdiI (see Figure 6A). Instead, the first catalytic turnover on YdiI was found to take place at the same rate as the ensuing turnovers, namely, 5.8 s^{-1}, which is comparable to the steady-state rate constant k_{cat} = 5.2 s^{-1}.[14]

For confirmation of this finding, a second method was used to monitor the catalytic turnovers. Specifically, [^{14}C]-benzoyl-CoA was used as substrate (the radiolabel facilitates precise quantitation of the reaction solution components) in conjunction with rapid acid-quench and HPLC chromatographic techniques. The acid-quench denatures the protein, thereby releasing product and unconsumed substrate. If the mixed anhydride is present, it is expected to undergo hydrolysis in the quench solution, releasing [^{14}C]-benzoic acid to the product pool. The [^{14}C]-benzoic acid and the unconsumed [^{14}C]-benzoyl-CoA were separated, and the level of radioactivity in each fraction was measured. The time courses determined for the reactions carried out using two different ratios of enzyme to substrate (1:2.5 and 1:12.5) showed the same result, which is no "burst" phase associated with the first turnover (Figure 6B and C, respectively).

Taken together, these results indicate that the cleavage of the substrate thioester moiety occurs in a chemical step that is slower than the ensuing step(s), a finding that is consistent both with the general base catalysis mechanism and with the nucleophilic catalysis mechanism wherein the formation of the anhydride intermediate is rate-limiting.

Catalysis of a Single-Turnover Reaction in $H_2{}^{18}O$ Solvent. As illustrated in Scheme 2, the Glu63* base-catalyzed, single-turnover reaction of benzoyl-CoA in $H_2{}^{18}O$ solvent is predicted to proceed with incorporation of an ^{18}O into the carboxylate group of the benzoic acid product to form [^{18}O, ^{16}O]-benzoate. If, on the other hand, the Glu63* reacts with the benzoyl-CoA to form the mixed anhydride intermediate, and hydrolysis occurs at the Glu63* carbonyl carbon, the solvent ^{18}O atom will transfer to the Glu63* and the bridging ^{16}O atom of the anhydride will transfer to the benzoate to form [$^{16}O_2$]-benzoate. Conversely, attack of the $H_2{}^{18}O$ at the benzoyl carbonyl carbon of the mixed anhydride intermediate will form [^{18}O, ^{16}O]-benzoate as the product rather than [$^{16}O_2$]-benzoate

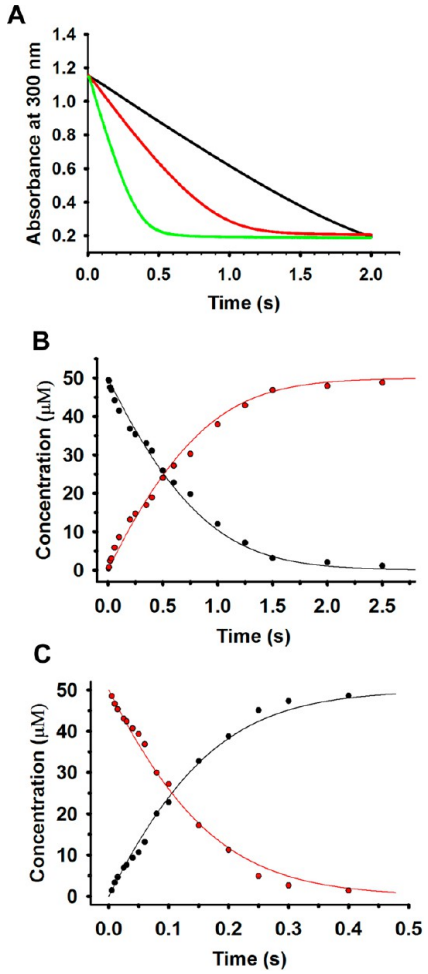

Figure 6. (A) Time courses for the hydrolysis of 100 μM 4-hydroxybenzoyl-CoA catalyzed by 10 μM (green), 16 μM (red), and 20 μM (black) YdiI in 50 mM K^+HEPES (pH 7.5) at 25 °C. Reactions were monitored at 300 nm using a stopped-flow spectrophotometer. (B) Time course for the YdiI (20 μM)-catalyzed hydrolysis of 50 μM [^{14}C]-benzoyl-CoA in 50 mM K^+HEPES (pH 7.5) at 25 °C; (black filled circles) concentration of [^{14}C]-benzoyl-CoA and (red filled circles) concentration of mixed ^{14}C-labeled anhydride intermediate and/or [^{14}C]-benzoate remaining in reaction solution upon the acid quench. (C) Same as in (B) except that 4 μM YdiI and 50 μM [^{14}C]-benzoyl-CoA were used.

(Scheme 2). Formation of the [$^{16}O_2$]-benzoate is thus diagnostic of the intermediacy of the mixed anhydride, whereas formation of [^{18}O, ^{16}O]-benzoate is consistent with general base catalysis as well as nucleophilic catalysis that proceeds via attack of the $H_2{}^{18}O$ at the benzoyl carbonyl carbon of the mixed anhydride intermediate.

Accordingly, a single-turnover reaction was carried out using a mixture of wild-type YdiI (889 μM) and benzoyl-CoA (750 μM) in 99.2% $H_2{}^{18}O$ at pH 7.5. The benzoic acid was isolated from the acid-quenched reaction mixture by solvent extraction and then subjected to mass spectral analysis. The mass spectrum of the benzoic acid standard, at natural isotopic abundance, is characterized by the parent ion (M*) peak at 122.1 m/z, parent ion fragment (M*−OH) peak at 105.1 m/z, and parent ion fragment (M*−COOH) at 77.1 m/z. The parent ion (M*) and parent ion fragment (M*−OH) were used as reporters of ^{18}O-incorporation from the $H_2{}^{18}O$ solvent. The mass spectrum (not shown) of the benzoic acid isolated

dx.doi.org/10.1021/bi500334v | *Biochemistry* 2014, 53, 4788−4805

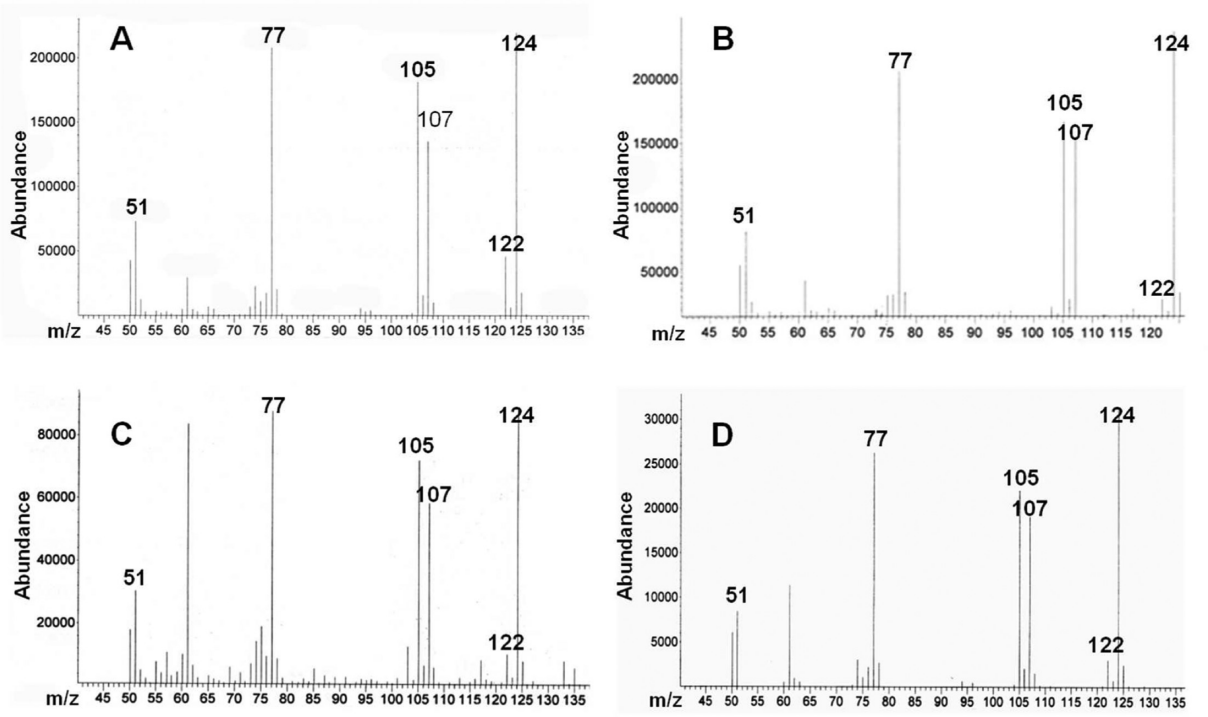

Figure 7. GC/MS spectra of benzoic acid samples isolated from the acid-quenched reaction mixtures generated from the incubation of benzoyl-CoA with wild-type or mutant YdiI in 99.2% $H_2{}^{18}O$ buffered at pH 7.5 and 25 °C with 50 mM K^+HEPES. Reaction solutions initially contained (A) 889 μM wild-type YdiI and 750 μM benzoyl-CoA; (B) 45 μM wild-type YdiI and 750 μM benzoyl-CoA; (C) 933 S67A* YdiI and 750 μM benzoyl-CoA; (D) 810 μM E63D* YdiI and 750 μM benzoyl-CoA.

from a control reaction, in which the enzyme was absent, was the same as that of the standard, thereby showing that the benzoic acid is not subject to isotopic exchange under these conditions. The mass spectrum of the benzoic acid isolated from the single-turnover reaction showed peaks 122.1 m/z ($[^{16}O_2]$-benzoic acid parent ion) and 124.1 m/z ($[^{18}O, {}^{16}O]$-benzoic acid parent ion) at a 1:5 ratio (20% ^{16}O-incorporation) (Figure 7A). The ratio of the parent ion fragment (M*−OH) peaks at 105.1 m/z and 107.1 m/z is 1.34:1.00. Similar results were obtained for experiments carried out in triplicate. The 17% $[^{16}O_2]$-benzoic acid observed for the single-turnover reaction is contrasted with the 4% $[^{16}O_2]$-benzoic acid observed for the multiple-turnover reaction of benzoyl-CoA (750 μM) catalyzed by wild-type YdiI (45 μM), for which 6% is the predicted maximum value. This result is analogous to that obtained previously for the *Ar* 4-HB-CoA TE, and it can be interpreted as evidence for the formation of a mixed anhydride intermediate. However, because we did not observe a burst phase associated with the first turnover in the multiple-turnover reaction time course, we cannot distinguish between nucleophilic catalysis coupled with preferred (not strict) regiochemistry of hydrolysis of the anhydride intermediate at the benzoyl carbonyl carbon versus competing mechanistic pathways in which Glu63* base catalysis dominates over Glu63* nucleophilic catalysis (see Scheme 2).

For the purpose of extending the comparison between YdiI and the *Ar* 4-HB-CoA TE, the single-turnover reaction in solvent $H_2{}^{18}O$ was carried out with the YdiI mutants S67A* and E63D*. The mass spectral data shown in Figure 7C and D define ratios of $[^{16}O_2]$-benzoic acid to $[^{18}O, {}^{16}O]$-benzoic acid equal to 1:9 and 1:12 (10% and 7.7% ^{16}O-incorporation into product), respectively. The reduction in ^{16}O-incorporation observed with the YdiI E63D* mutant is consistent with that observed of the *Ar* 4-HB-CoA TE E73D* mutant. In contrast, whereas the ^{16}O-incorporation observed with the YdiI S67A* mutant is decreased, it was increased for the *Ar* 4-HB-CoA TE T77A* mutant, thus indicating that the S67* and T77* contribute to catalysis differently.

Substrate Binding and Product Dissociation. The binding affinities of YdiI and YbdB toward the substrate benzoyl-CoA are approximated by the P-CoA competitive inhibition constants K_{is} = 7.8 ± 0.4 μM for YdiI and K_{is} = 65 ± 6 μM for YbdB (Table 2). The X-ray crystallographic structures of the YdiI·(P-CoA) and YbdB·(P-CoA) complexes show that the orientation of P-CoA is such that only the CoA moiety has access to solvent. An analogous scenario is indicated by the X-ray structure of the homolog *Ar* 4-HB-CoA TE in complex with 4-hydroxyphenacyl-CoA.[3] Based on structural data alone, one would predict ordered product release, with CoA departure occurring first. Indeed, in earlier work, this prediction was verified for the *Ar* 4-HB-CoA TE by demonstrating non-competitive (mixed-type) product inhibition for CoA (K_{is} = 16 ± 2 μM, K_{ii} = 29 ± 2 μM) and competitive product inhibition for 4-hydroxybenzoate (K_{is} = 240 ± 80 μM).[28] In the present work, CoA was also shown to be a noncompetitive product inhibitor of YbdB-catalyzed benzoyl-CoA hydrolysis (K_{is} = 210 ± 10 μM, K_{ii} = 1130 ± 100 μM) (Figure SI9A, Supporting Information; Table 2); however, for YdiI, competitive inhibition by CoA was observed (K_{is} = 16 ± 1 μM) (Figure SI9B, Supporting Information; Table 2). Competitive inhibition is consistent with ordered product release only if the dissociation of CoA follows that of benzoic acid. The release of benzoic acid from the YdiI ternary product complex could occur providing that the aryl/alkyl group-binding pocket opens to solvent. Although the binding site is largely closed in the X-ray crystal structure of the YdiI·(P-CoA) complex (Figure 2B),

dx.doi.org/10.1021/bi500334v | *Biochemistry* 2014, 53, 4788−4805

it is open in the structure of the YdiI·(UDO-CoA) complex (Figure 2A), thus suggesting that release of benzoic acid before CoA release might be possible.

Rate-Limiting Chemistry. The apparent rate constant (k_{obs}) governing the catalytic turnover of YdiI·(benzoyl-CoA) to YdiI·(CoA)(benzoic acid) was determined for the reaction of 20 μM [^{14}C]-benzoyl-CoA with 50 μM YdiI at pH 7.5 and 25 °C. The time course for the single-turnover reaction (Figure 8) was fitted by iterative curve simulation using the reaction

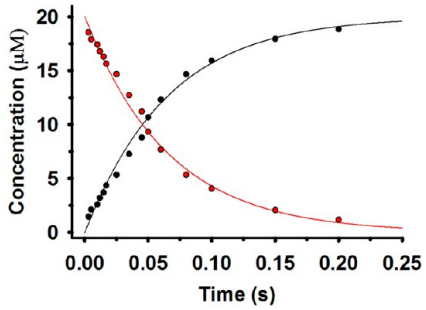

Figure 8. YdiI (50 μM) catalyzed single-turnover reaction of [^{14}C]-benzoyl-CoA (20 μM) in 50 mM K$^+$HEPES (pH 7.5) at 25 °C; (black filled circles) concentration of [^{14}C]-benzoyl-CoA and (red filled circles) concentration of mixed ^{14}C-labeled anhydride intermediate and/or [^{14}C]-benzoate remaining in reaction solution upon rapid acid quench.

sequence YdiI + benzoyl-CoA ↔ YdiI·(benzoyl-CoA) → YdiI·(CoA)(benzoic acid) in conjunction with the KinTek Corporation Global Kinetic Explorer software[34] to define the benzoyl-CoA k_{on} = 50−125 μM^{-1}·s^{-1} and k_{off} = 400−650 s^{-1}, and for the chemical step(s) k_{obs} = 15−19 s^{-1}. The steady-state k_{cat} = 18 s^{-1} is in agreement with the range of values defined for k_{obs}. Taken together, the values of the microscopic rate constants (indicating that substrate binding is not rate-limiting), the absence of a "burst" phase associated with the first turnover in the presteady-state multiple-turnover time course (Figure 6), and the observed normal solvent (H_2O vs D_2O) isotope effect on k_{cat} ($^Hk_{cat}/^Dk_{cat}$ = 1.9 ± 0.1 for YdiI and $^Hk_{cat}/^Dk_{cat}$ = 2.2 ± 0.1 for YbdB) show that the chemistry, rather than substrate binding or product release, is rate-limiting.

Divergence of Structural Determinants of Catalysis and Biological Function in YbdB and YdiI. In this section, we compare YbdB to YdiI to identify key differences in structure that support functional divergence. Next, we contrast the divergence in structure−function between YbdB and YdiI to that with the evolutionarily more distant *Ar* 4-HB-CoA thioesterase. X-ray crystallographic structures of this homolog[3] as well its mechanisms of substrate recognition and catalysis[28] have been detailed in previous reports.

Substrate Recognition. The respective physiological thioester substrates targeted by YdiI and YbdB,[14−19] namely, 1,4-dihydroxynapthoyl-CoA and (hydroxy)benzoyl-*holo*EntB, differ both in the structure of the appendage to the phosphopantetheine thiol moiety (viz., adenosine-3′, 5′-diphosphate vs the ACP domain of EntB) and in the structure of the organic acid moiety (1,4-dihydroxynapthoic acid vs (hydroxy)benzoic acid). The narrow channel, which leads from the protein surface to the site of catalysis, binds the phosphopantetheine moiety using desolvation and weak electrostatic forces derived from close packing to augment the two hydrogen bonds derived from backbone amide groups (Figure 4A). Thus, tight binding of the phosphopantetheine moiety is preserved despite the differences in YbdB and YdiI sequence that exist in this region (Figure 4A).

The adenosine-3′,5′-diphosphate unit of the CoA thioester and the ACP domain of the *holo*EntB thioester are accommodated by the protein surface formed at the interface of three of the four subunits that comprise the dimer of dimers (Figure 3A). Whereas the YbdB and YdiI main chain conformations in this region are quite similar, the steric and electrostatic topological features of the surface are not (Figure 3C), and this is because of the divergence in the sequence in this region (Figure 3B). YbdB has evolved recognition of the ACP domain in EntB while maintaining compatibility with the adenosine-3′,5′-diphosphate moiety of CoA. Simple inspection of the interacting surfaces does not reveal the nature of the protein−protein interaction, and thus far, our attempts to crystallize the complex have not been successful.

Unlike the case of YdiI, the substrate range of YbdB does not include fatty acyl-CoA thioesters or 1,4-dihydroxynaphthyl-CoA.[14] Such a divergence in substrate recognition might be attributed to the observed differences in the residues that form the respective alkyl/aryl unit-binding sites. Of special interest is the Val68 residue in YdiI, which is replaced by the larger Met68 in YbdB (Figure 5B; Figure SI8, Supporting Information). In the companion paper,[14] we reported a ∼50-fold increase in the k_{cat}/K_m value for YbdB M68V-catalyzed 1,4-dihydroxynapthoyl-CoA hydrolysis compared to that of wild-type YbdB, and a ∼10-fold increase in k_{cat}/K_m value for YbdB M68V-catalyzed lauroyl-CoA hydrolysis. The additional space in the YbdB aryl/alky group binding site gained by the mutation is one possible explanation for the increased activity with the larger substrates. An alternative possibility is that the replacement of the Met68 with Val reduces the packing of the hydrophobic side chains in the binding site, and this in turn promotes the open conformation observed in the structure of the wild-type YdiI·(UDO-CoA) complex (Figure 2A; Figure SI9, Supporting Information). As we pointed out,[14] there exists a high (although not 100%) correlation of the occurrence of Met68 with the predicted YbdB proofreader function in the enterobactin pathway and of Val68 with the predicted YdiI 1,4-DHN-CoA thioesterase function in the menaquinone pathway.

YbdB, YdiI, and the *Ar* 4-HB-CoA TE share high catalytic efficiency toward the metabolite 4-hydroxybenzoyl-CoA, as is demonstrated by their respective k_{cat}/K_m values of 7 × 10^4, 6 × 10^5, and 5 × 10^7 M^{-1}·s^{-1}.[8,14] Whereas the k_{cat} values for all three homologs are similar (5, 2, and 7 s^{-1}, respectively), the K_m value for the *Ar* 4-HB-CoA thioesterase is significantly lower (21, 9, and 0.1 μM, respectively). The inhibition constants indicate ∼10-fold tighter CoA binding to YdiI (K_{is} = 16 μM) (Table 2) and to the *Ar* 4HB-CoA TE (K_{is} = 29 μM)[28] than CoA binding to YbdB (K_{is} = 210 μM) (Table 2). The three residues that are responsible for desolvation of the substrate pantetheine moiety in YbdB match those in the *Ar* 4-HB-CoA TE, whereas YdiI possesses a Ser92 in place of the YbdB Pro92 (Figure 4A) or the *Ar* 4-HB-CoA TE Pro103 (Figure 9A). The CoA adenosine 3′,5′-diphosphate binding region also contains residues that the *Ar* 4-HB-CoA TE shares with one (Ser120 with Ser109) or both (Arg102 with Arg135, Arg102 with Arg91, and His117 with His106) of the homologs (Figures 3B and 9A). In view of the low overall sequence identity between the *Ar* 4-HB-CoA TE and the two paralogs, the similarities in their CoA-binding sites are striking.

The region of the *Ar* 4-HB-CoA TE that has undergone considerable specialization for divergence of function is the

dx.doi.org/10.1021/bi500334v | *Biochemistry* 2014, 53, 4788−4805

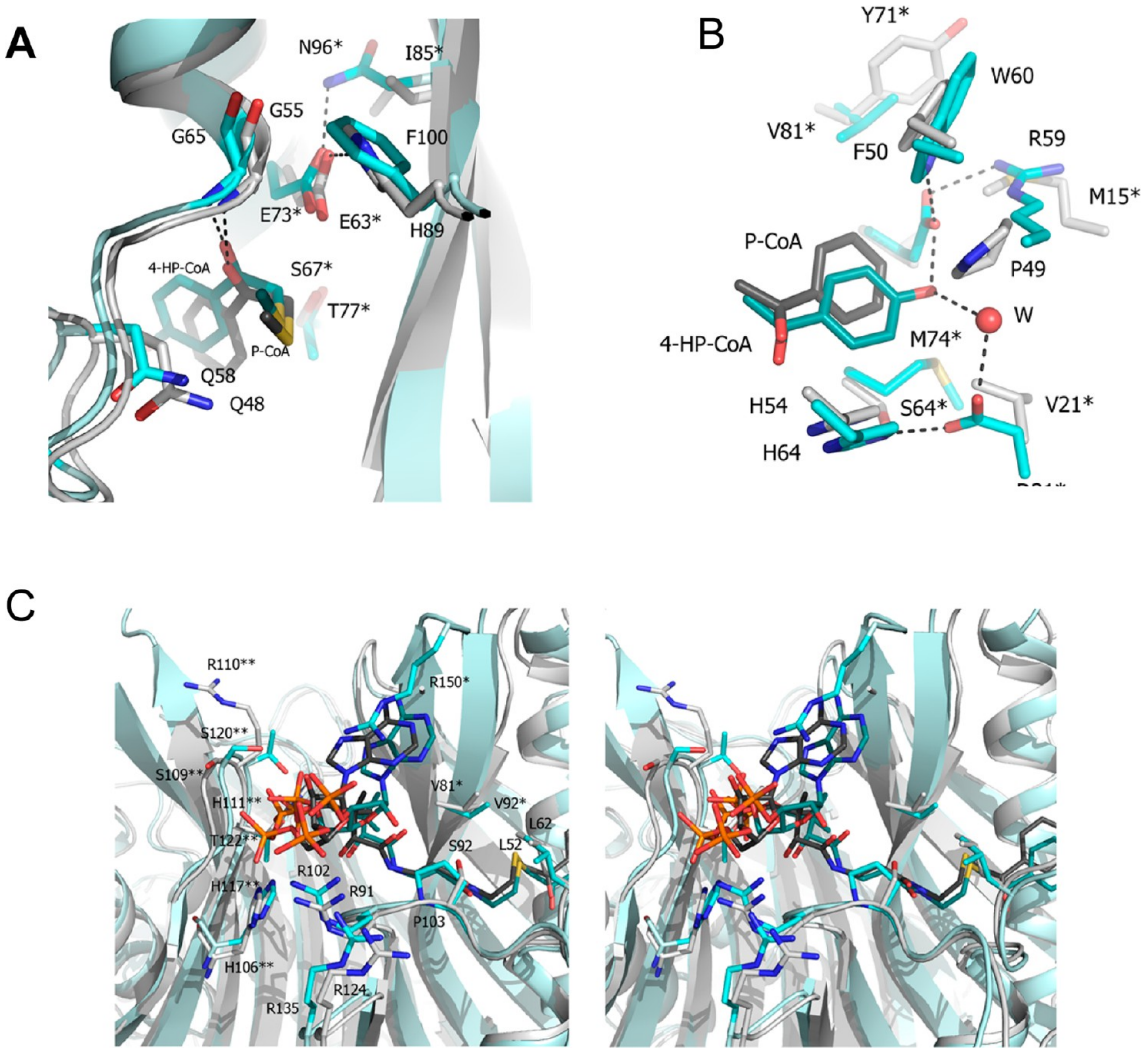

Figure 9. Pymol representation of the superposition of the *Arthrobacter* sp. strain AU 4-hydroxybenzoyl-CoA thioesterase bound with 4-hydroxyphenacyl-CoA and YdiI bound with phenacyl-CoA (carbon atoms colored cyan or gray, respectively, and oxygen atoms are red, nitrogen atoms blue, phosphorus atoms orange, and sulfur atoms yellow). Ligands (truncated in (A) and (B)) and side chains are shown in stick. Hydrogen bonds are represented by dashed-lines. (A) Comparison of the catalytic sites. (B) Stereo figure made in Pymol Comparison of the aryl group-binding sites. The ordered water molecule is shown as a red sphere. (C) Comparison of the CoA binding sites.

aryl/alkyl moiety binding site (Figure 9B). The function of the 4-HB-CoA TE in the 4-chlorobenzoate degradation pathway[7] dictates that the thioesterase discriminates between the first pathway intermediate 4-chlorobenzoyl-CoA (4-CB-CoA) and its product, 4-HB-CoA, with high efficiency.[8] Indeed, there is a ~10 000 difference in k_{cat}/K_m values that derives from a comparatively smaller 4-CB-CoA k_{cat} value (0.25 s^{-1}) and a much larger K_m value (113 μM).[8] The k_{cat}/K_m value for benzoyl-CoA (8×10^3 $M^{-1}\cdot s^{-1}$) is also ~10 000-fold smaller than that for 4-HB-CoA owing, primarily, to the large K_m value (240 μM).[8] In contrast, YbdB and YdiI do not select the ring C(4)OH as indicated by the observation that benzoyl-CoA and 4-HB-CoA are equally active substrates.[14] The special tailoring of the *Ar* 4-HB-CoA TE aryl group-binding site for optimal 4-HB-CoA binding includes the engagement of the ring C(4)OH in an extensive hydrogen-bond network (see Figure 9B).[3,14] In contrast, the aryl group binding sites of YbdB and YdiI are largely nonpolar, and the respective crystal structures of the respective 2,4-DHP-CoA complexes indicate that the C(4)OH does not form a hydrogen with a binding site residue (Figure 5C).

Catalytic Mechanism. The key residues that form the catalytic site in YbdB and YdiI are stringently conserved (Figure 4B). The catalytic site residues of YbdB and YdiI are matched with their positional counterparts in the catalytic site of *Ar* 4-HB-CoA TE (Figure 9C), save three notable exceptions. Specifically, the His89 of YbdB and YdiI, which functions (via hydrogen-bond formation) to orient the catalytic carboxylate residue (Glu63*), is replaced with Phe100 in the *Ar* 4-HB-CoA TE. The catalytic carboxylate residue (Glu73*) of the *Ar* 4-HB-CoA TE is instead oriented through hydrogen-bond formation with Asn96*, which is located on the subunit opposite of that which contributes the His89 in YbdB and YdiI (Figure 9A). The counterpart to the *Ar* 4-HB-CoA TE Asn96* is Leu85* in YbdB and Ile85* in YdiI. Despite the difference in the locations of the respective hydrogen-bond donors, the orientation of the Glu73* carboxylate group in the *Ar* 4-HB-CoA TE is the same as that observed for the corresponding Glu63* carboxylate groups in YbdB and YdiI (Figures 9A and 4B). Likewise, the Thr77* and Gln78 of the *Ar* 4-HB-CoA TE and the Ser67* and Gln58 of YbdB and YdiI occupy the same positions in the respective catalytic sites. Despite the similar positioning of

dx.doi.org/10.1021/bi500334v | *Biochemistry* 2014, 53, 4788−4805

these residues, the experimental probes (viz., transient kinetics and ^{18}O-solvent labeling) originally used to define the catalytic mechanism of *Ar* 4-HB-CoA TE[28] proved to be less effective when applied to YdiI catalysis. Indeed, it is not clear that Glu63* functions as nucleophile only, or that a competing pathway exists in which it functions as general base (Scheme 2).

CONCLUSION

What have we learned with regard to the evolution of substrate recognition from this comparative analysis? First, we have shown that YdiI and YbdB, and their distant relative *Ar* 4-HB-CoA TE, have retained the CoA-binding site inherited from an ancient (type AB[b]) clade member, and that this recognition motif has been conserved in YbdB despite the divergence in structure which underlies *holo*EntB recognition. Although the respective interaction surfaces of the EntB ACP domain with EntD and EntF have been described,[35,36] the EntB ACP−YbdB interface has yet to be defined.[c] Second, it is evident that the divergence in the aryl-group binding site is the basis for the divergence in substrate specificity that supports the diverse set of biological functions acquired by these three homologs. Third, the multitasking aryl group binding site discovered in YdiI (viz., recognition of fatty acyl-CoA as well as aryl-CoA metabolites) is quite intriguing and warrants further investigation.

What have we learned about the adaptation of the catalytic mechanism with evolving substrate recognition? The take-home lesson is that inherent in the catalytic scaffold of any given hotdog-fold thioesterase is the potential for catalyzed hydrolysis via a single-step, general base catalysis pathway and a two-step, nucleophilic catalysis pathway. We speculate further that the energy profiles for the competing reaction coordinates are differentiated by subtle differences in local, and possibly global, residue usage. And thus, along with the sequence divergence that accompanies the evolution of a new function is the divergence of catalytic mechanism employed by a conserved constellation of catalytic residues. A small shift in the position of the substrate thioester group relative to the catalytic carboxylate group caused by a switch in the structure of the physiological substrate might be most readily accommodated by the switch from nucleophilic catalysis to base catalysis or vice versa.

ASSOCIATED CONTENT

Supporting Information

Protocols for preparation of the [^{14}C]-benzoyl-CoA, 2,4-dihydroxyphenacyl-CoA, and phenacyl-CoA. Figures SI1−SI9, which depict X-ray crystallographic electron density maps, Lineweaver−Burk plots of inert substrate analogs and product inhibitors, and Pymol-generated YbdB and YdiI structures. This material is available free of charge via the Internet at http://pubs.acs.org.

Accession Codes

The *Escherichia coli* YbdB and YdiI coordinates and structure factors have been submitted to the PDB with accession codes as follows: YbdB in complex with 2,4-dihydroxyphenacyl-CoA (4K4D) or phenacyl-CoA (4K4C); YdiI in complex with 2,4-dihydroxyphenacyl-CoA (4K49), phenacyl-CoA (4K4A), or undecan-2-one-CoA (4K4B).

AUTHOR INFORMATION

Corresponding Authors

*(K.N.A., for correspondence regarding X-ray structure determinations.) Mailing address: 590 Commonwealth Ave, Room 299, Boston, MA 02215. Tel: 617-358-5544. Fax: 202-354-5386. E-mail: drkallen@bu.edu.

*(D.D.-M., for correspondence regarding biochemical investigations.) Tel: 505-277-3383. Fax: 505-277-2609. E-mail: dd39@unm.edu.

Author Contributions

§R.W. (structure) and J.A.L. (catalysis) share first authorship.

Funding

This work was supported by NIH Grant R01-GM 28688.

Notes

The authors declare no competing financial interest.

ABBREVIATIONS

*holo*ACP, phosphopantetheine-modified acyl carrier protein; CoA, coenzyme A; 4-HB-CoA, 4-hydroxybenzoyl-coenzyme A; *Ar*, *Arthrobacter* special strain AU; *Ps*, *Pseudomonas* special strain CBS3; P-CoA, phenacyl-coenzyme A; 2,4-DHP-CoA, 2,4-dihydroxyphenacyl-CoA; UDO-CoA, undecan-2-one-coenzyme A; 4-HP-CoA, 4-hydroxyphenacyl-coenzyme A; DTNB, 5,5′-dithio-bis(2-nitrobenzoic acid); SDS-PAGE, sodium dodecyl sulfate polyacrylamide gel electrophoresis; GC/MS, gas chromatographic/mass spectrometric; HEPES, 2-[4-(2-hydroxyethyl)piperazin-1-yl]ethanesulfonic acid; DTT, dithiothreitol

ADDITIONAL NOTES

[a]In this paper, the term "*holo*" is used to specify that the ACP serine residue is functionalized with a phosphopantetheinyl group. Also, the term "(hydroxy)benzoyl" is used in a generic sense to signify that the organic acid unit of the thioester is benzoic acid or a benzoic acid adduct that possesses one or two ring hydroxyl groups.

[b]For ease of referencing, the *Pseudomonas* thioesterase clade has been named "type AA" to signify that the active site catalytic carboxylate residue and the thioester-polarizing α-helix N-terminus residue are contributed by the same subunit of the functional dimer.[1,2] The *Arthrobacter* thioesterase clade was named "type AB" because these two active site residues are located on the opposing subunits of the dimer.[3]

[c]To date, our attempts at generating crystals of YbdB in complex with undecan-one-CoA have not been successful.

[d]The respective tetrahedral oxyanion intermediates associated with substitution at an acyl carbonyl carbon are not included in this model because thioesters and anhydrides, owing to their low-energy anionic leaving groups (viz., thiolate anion and carboxylate anion, respectively), are reported to undergo concerted nucleophilic substitution reactions rather than follow the classical addition−elimination pathway.[4]

REFERENCES

(1) Benning, M. M., Wesenberg, G., Liu, R., Taylor, K. L., Dunaway-Mariano, D., and Holden, H. M. (1998) The three-dimensional structure of 4-hydroxybenzoyl-CoA thioesterase from *Pseudomonas* sp. Strain CBS-3. *J. Biol. Chem. 273*, 33572−335979.

(2) Thoden, J. B., Holden, H. M., Zhuang, Z., and Dunaway-Mariano, D. (2002) X-ray crystallographic analyses of inhibitor and substrate complexes of wild-type and mutant 4-hydroxybenzoyl-CoA thioesterase. *J. Biol. Chem. 277*, 27468−27476.

(3) Thoden, J. B., Zhuang, Z., Dunaway-Mariano, D., and Holden, H. M. (2003) The structure of 4-hydroxybenzoyl-CoA thioesterase from *Arthrobacter* sp. strain SU. *J. Biol. Chem. 278*, 43709−43716.
(4) Hess, R. A., Hengge, A. C., and Cleland, W. W. (1998) Isotope Effects on Enzyme-Catalyzed Acyl Transfer from p-Nitrophenyl Acetate: Concerted Mechanisms and Increased Hyperconjugation in the Transition State. *J. Am. Chem. Soc. 120*, 2703−2709.
(5) Leesong, M., Henderson, B. S., Gillig, J. R., Schwab, J. M., and Smith, J. L. (1996) Structure of a dehydratase-isomerase from the bacterial pathway for biosynthesis of unsaturated fatty acids: Two catalytic activities in one active site. *Structure 4*, 253−264.
(6) Scholten, J. D., Chang, K. H., Babbitt, P. C., Charest, H., Sylvestre, M., and Dunaway-Mariano, D. (1991) Novel enzymic hydrolytic dehalogenation of a chlorinated aromatic. *Science 253*, 182−185.
(7) Schmitz, A., Gartemann, K. H., Fiedler, J., Grund, E., and Eichenlaub, R. (1992) Cloning and sequence analysis of genes for dehalogenation of 4-chlorobenzoate from *Arthrobacter* sp. strain SU. *Appl. Environ. Microbiol. 58*, 4068−4071.
(8) Zhuang, Z., Gartemann, K. H., Eichenlaub, R., and Dunaway-Mariano, D. (2003) Characterization of the 4-hydroxybenzoyl-coenzyme A thioesterase from Arthrobacter sp. strain SU. *Appl. Environ. Microbiol. 2003* (69), 2707−2711.
(9) Cao, J., Xu, H., Zhao, H., Gong, W., and Dunaway-Mariano, D. (2009) The mechanisms of human hotdog-fold thioesterase 2 (hTHEM2) substrate recognition and catalysis illuminated by a structure and function based analysis. *Biochemistry 48*, 1293−1304.
(10) Song, F., Zhuang, Z., Finci, L., Dunaway-Mariano, D., Kniewel, R., Buglino, J. A., Solorzano, V., Wu, J., and Lima, C. D. (2006) Structure, function, and mechanism of the phenylacetate pathway hot dog-fold thioesterase PaaI. *J. Biol. Chem. 281*, 11028−11038.
(11) Wang, M., Song, F., Wu, R., Allen, K. N., Mariano, P. S., and Dunaway-Mariano, D. (2013) Co-evolution of HAD phosphatase and hotdog-fold thioesterase domain function in the menaquinone-pathway fusion proteins BF1314 and PG1653. *FEBS Lett. 587*, 2851−2859.
(12) Zhao, H., Martin, B. M., Bisoffi, M., and Dunaway-Mariano, D. (2009) The Akt C-terminal modulator is an acyl-CoA thioesterase of the hotdog-fold thioesterase family. *Biochemistry 48*, 5507−5509.
(13) Khersonsky, O., and Tawfik, D. S. (2010) Enzyme promiscuity: a mechanistic and evolutionary perspective. *Annu. Rev. Biochem. 79*, 471−505.
(14) Latham, J. A., Chen, D., Allen, K. N., and Dunaway-Mariano, D. (2014) Divergence of Substrate Specificity and Function in the *Escherichia coli* Hotdog-fold Thioesterase Paralogs YdiI and YbdB. *Biochemistry*, DOI: 10.1021/bi500333m.
(15) Latham, J. A. (2012) Structure to function: Case studies of hotdog-fold superfamily thioesterases from *Escherichia coli*. PhD Thesis, University of New Mexico, pp 2−96.
(16) Chen, M., Ma, X., Chen, X., Jiang, M., Song, H., and Guo, Z. (2013) Identification of a hotdog fold thioesterase involved in the biosynthesis of menaquinone in *Escherichia coli*. *J. Bacteriol. 195*, 2768−2775.
(17) Leduc, D., Battesti, A., and Bouveret, E. (2007) The hotdog thioesterase EntH (YbdB) plays a role in vivo in optimal enterobactin biosynthesis by interacting with the ArCP domain of EntB. *J. Bacteriol. 189*, 7112−7126.
(18) Chen, D., Wu, R., Bryan, T. L., and Dunaway-Mariano, D. (2009) In vitro kinetic analysis of substrate specificity in enterobactin biosynthetic lower pathway enzymes provides insight into the biochemical function of the hot dog-fold thioesterase EntH. *Biochemistry 48*, 511−513.
(19) Guo, Z.-F., Sun, Y., Zheng, S., and Guo, Z. (2009) Preferential hydrolysis of aberrant intermediates by the type II thioesterase in Escherichia coli nonribosomal enterobactin synthesis: substrate specificities and mutagenic studies on the active site residues. *Biochemistry 48*, 1712−1722.
(20) Luo, L., Taylor, K. L., Xiang, H., Wei, Y., Zhang, W., and Dunaway-Mariano, D. (2001) Role of active site binding interactions in 4-chlorobenzoyl-coenzyme A dehalogenase catalysis. *Biochemistry 40*, 15684−15692.
(21) Bradford, M. M. (1976) A rapid and sensitive method for the quantitation of microgram quantities of protein utilizing the principle of protein-dye binding. *Anal. Biochem. 72*, 248−254.
(22) Otwinowski, Z., and Minor, W. (1997) Processing of X-ray Diffraction Data Collected in Oscillation Mode. *Methods Enzymol. 276*, 307−326.
(23) Potterton, E., Briggs, P., Turkenburg, M., and Dodson, E. (2003) A graphical user interface to CCP4 program suite. *Acta Crystallogr., Sect. D: Biol. Crystallogr. 59*, 1131−1137.
(24) Badger, J., Sauder, J. M., Adams, J. M., Antonysamy, S., Bain, K., Bergseid, M. G., Buchanan, S. G., Buchanan, M. D., Batiyenko, Y., Christopher, J. A., Emtage, S., Eroshkina, A., Feil, I., Furlong, E. B., Gajiwala, K. S., Gao, X., He, D., Hendle, J., Huber, A., Hoda, K., Kearins, P., Kissinger, C., Laubert, B., Lewis, H. A., Lin, J., Loomis, K., Lorimer, D., Louie, G., Maletic, M., Marsh, C. D., Miller, I., Molinari, J., Muller-Dieckmann, H. J., Newman, J. M., Noland, B. W., Pagarigan, B., Park, F., Peat, T. S., Post, K. W., Radojicic, S., Ramos, A., Romero, R., Rutter, M. E., Sanderson, W. E., Schwinn, K. D., Tresser, J., Winhoven, J., Wright, T. A., Wu, L., Xu, J., and Harris, T. J. (2005) Structural analysis of a set of proteins resulting from a bacterial genomics project. *Proteins 60*, 787−796.
(25) Adams, P. D., Grosse-Kunstleve, R. W., Hung, L. W., Ioerger, T. R., McCoy, A. J., Moriarty, N. W., Read, R. J., Sacchettini, J. C., Sauter, N. K., and Terwilliger, T. C. (2002) PHENIX: Building new software for automated crystallographic structure determination. *Acta Crystallogr., Sect. D: Biol. Crystallogr. 58*, 1948−1954.
(26) Emsley, P., and Cowtan, K. (2004) Coot: Model-building tools for molecular graphics. *Acta Crystallogr., Sect. D: Biol. Crystallogr. 60*, 2126−2132.
(27) Laskowski, R. A., MacArthur, M. W., Moss, D. S., and Thornton, J. M. (1993) PROCHECK - A program to check the stereochemical quality of protein structures. *J. Appl. Crystallogr. 26*, 283−291.
(28) Song, F., Thoden, J. B., Zhuang, Z., Latham, J., Trujillo, M., Holden, H. M., and Dunaway-Mariano, D. (2012) The Catalytic Mechanism of the Hotdog-fold Enzyme Superfamily 4-Hydroxybenzoyl-CoA Thioesterase from *Arthrobacter* sp. Strain SU. *Biochemistry 51*, 7000−7016.
(29) Dong, J., Zhuang, Z., Song, F., Dunaway-Mariano, D., and Carey, P. C. (2012) A Thioester Substrate Binds to the Enzyme *Arthrobacter* Thioesterase in Two Ionization States; Evidence from Raman Difference Spectroscopy. *J. Raman Spectrosc. 43*, 65−71.
(30) Zhuang, Z., Song, F., Zhang, W., Taylor, K., Archambault, A., Dunaway-Mariano, D., Dong, J., and Carey, P. R. (2002) Kinetic, Raman, NMR, and site-directed mutagenesis studies of the *Pseudomonas* sp. strain CBS3 4-hydroxybenzoyl-CoA thioesterase active site. *Biochemistry 41*, 11152−11160.
(31) Zhuang, Z., Latham, J., Song, F., Zhang, W., Trujillo, M., and Dunaway-Mariano, D. (2012) Investigation of the Catalytic Mechanism of the Hotdog-Fold Enzyme Superfamily Pseudomonas sp. Strain CBS3 4-Hydroxybenzoyl-CoA Thioesterase. *Biochemistry 51*, 786−794.
(32) Dong, J., Luo, L., Liang, P., Dunaway-Mariano, D., and Carey, P. (2000) Raman difference spectroscopic studies of dithiobenzoyl substrate and product analogs binding to the enzyme dehologenase: pi-electron polarization is prevented by C═O to C═S substitution. *J. Raman Spectrosc. 31*, 365−371.
(33) Lightstone, F. C., and Bruice, T. C. (1996) Ground state conformations and entropic and enthalpic factors in the efficiency of intramolecular and enzymic reactions. 1. Cyclic anhydride formation by substituted glutarates, succinate, and 3,6-endoxo-D4-tetrahydrophthalate monophenyl esters. *J. Am. Chem. Soc. 118*, 2595−2605.
(34) Johnson, K. A. (2009) Fitting enzyme kinetic data with KinTek Global Kinetic Explorer. *Methods Enzymol. 467*, 601−626.
(35) Lai, J. R., Fischbach, M. A., Liu, D. R., and Walsh, C. T. (2006) Localized protein interaction surfaces on the EntB carrier protein revealed by combinatorial mutagenesis and selection. *J. Am. Chem. Soc. 128*, 11002−11003.

(36) Lai, J. R., Fischbach, M. A., Liu, D. R., and Walsh, C. T. (2006) A protein interaction surface in nonribosomal peptide synthesis mapped by combinatorial mutagenesis and selection. *Proc. Nat. Acad. Sci. U.S.A. 103,* 5314−5319.